NPS67-85-011CR

NAVAL POSTGRADUATE SCHOOL

Monterey, California

CONTRACTOR REPORT

INVESTIGATION OF THE INTERACTION BETWEEN THE ROTOR AND STATOR OF A TRANSONIC COMPRESSOR

F. NEUHOFF

ae EXOTECH, INC. TR-8503
3935 BEACON AVE, SUITE D
FREMONT, CA 94538-1405

NOVEMBER 1985

FINAL REPORT FOR PERIOD MAY 1985 - NOVEMBER 1985

Prepared for:
Naval Postgraduate School
Monterey, CA 93943

NAVAL POSTGRADUATE SCHOOL
Monterey, California

Rear Admiral R. H. Shumaker
Superintendent

D. A. Schrady
Provost

A small transonic axial air compressor and methods for measuring performance and detailed internal (unsteady) flow behavior have been developed in a program conducted at the Turbopropulsion Laboratory of the Naval Postgraduate School. The present work was completed under contract N62271-85-M-0423 issued under Work Request N6237685WR00018.

The program monitor at the Naval Air Propulsion Center was M. Dell (PE31).

This report was prepared by:

UNCLASSIFIED
CURITY CLASSIFICATION OF THIS PAGE

REPORT DOCUMENTATION PAGE

b. REPORT SECURITY CLASSIFICATION UNCLASSIFIED	1b RESTRICTIVE MARKINGS
b. SECURITY CLASSIFICATION AUTHORITY	3. DISTRIBUTION / AVAILABILITY OF REPORT Approved for Public Release; distribution is unlimited
b. DECLASSIFICATION / DOWNGRADING SCHEDULE	
PERFORMING ORGANIZATION REPORT NUMBER(S) TR 8503	5. MONITORING ORGANIZATION REPORT NUMBER(S) NPS67 - 85 - 011CR
a. NAME OF PERFORMING ORGANIZATION Exotech Inc. — 6a. OFFICE SYMBOL (If applicable)	7a. NAME OF MONITORING ORGANIZATION Naval Postgraduate School
. ADDRESS (City, State, and ZIP Code) 3935 Beacon Ave., Ste. D, Fremont, California 94538-1405	7b. ADDRESS (City, State, and ZIP Code) Monterey, California 93943-5000
a. NAME OF FUNDING / SPONSORING ORGANIZATION Office of Naval Research — 8b OFFICE SYMBOL (If applicable)	9. PROCUREMENT INSTRUMENT IDENTIFICATION NUMBER N00014 - 85 - C - 0676/N6237685WR00018
c. ADDRESS (City, State, and ZIP Code) Arlington, Virginia 22217	10. SOURCE OF FUNDING NUMBERS

PROGRAM ELEMENT NO.	PROJECT NO.	TASK NO.	WORK UNIT ACCESSION NO.
61153N	RR024	03	01

1. TITLE (Include Security Classification)

INVESTIGATION OF THE INTERACTION BETWEEN THE ROTOR AND STATOR OF A TRANSONIC COMPRESSOR

2. PERSONAL AUTHOR(S) F. NEUHOFF

3a. TYPE OF REPORT	13b. TIME COVERED	14. DATE OF REPORT (Year, Month, Day)	15 PAGE COUNT
Final	FROM May 85 TO Nov 85	851130	55

6. SUPPLEMENTARY NOTATION

7 COSATI CODES			18. SUBJECT TERMS (Continue on reverse if necessary and identify by block number)
FIELD	GROUP	SUB-GROUP	Rotor Stator Matching Turbomachinery Flow Fields Experimental Evaluation, Flow Calculations

9. ABSTRACT (Continue on reverse if necessary and identify by block number)

An evaluation of the rotor outflow matching to a downstream stator was conducted for a transonic compressor stage. The study compared experimental data and throughflow computations of the blading flow field to examine the flow angles and velocity distribution of the isolated rotor and the stage. An assessment of the data allowed the degree of interaction and matching of the blade rows to be determined. It was found that the rotor flow was only slightly modified by the presence of the stator and that the rotor flow dominated the overall stage performance.

0 DISTRIBUTION / AVAILABILITY OF ABSTRACT	21. ABSTRACT SECURITY CLASSIFICATION
☒ UNCLASSIFIED/UNLIMITED ☐ SAME AS RPT. ☐ DTIC USERS	UNCLASSIFIED
2a NAME OF RESPONSIBLE INDIVIDUAL R. P. SHREEVE	22b. TELEPHONE (Include Area Code) (408) 646-2593 — 22c. OFFICE SYMBOL 67Sf

DD FORM 1473, 84 MAR — 83 APR edition may be used until exhausted. All other editions are obsolete

SECURITY CLASSIFICATION OF THIS PAGE

☆ U.S. Government Printing Office: 1986—606-24.

UNCLASSIFIED

TABLE OF CONTENTS

LIST OF FIGURES

LIST OF FIGURES

LIST OF TABLES

I. INTRODUCTION

This report discusses the matching of rotor and stator flow in a transonic compressor stage used for experimental measurement technique development. The compressor is a small (11 inches in diameter), single stage axial machine with a design stage pressure ratio of about 1.5 at 30,460 RPM (Fig. 1). The design was completed in the late 1960's by Dr. M. Vavra and is documented in Ref. 1. The compressor does not reflect today's state of the art of high speed compressor technology. It is, however, a valuable tool to investigate phenomena peculiar to transonic flows such as shock systems and the losses accompanied with them.

Initial testing, aimed at establishing the overall performance map of this compressor, revealed that the flow into the rotor was in disagreement with the design. The flow rate at the full open throttle condition was too small and the radial distribution of velocity did not match the rotor requirements. In Fig. 2 the measured relative rotor inlet angle β_1 and rotor incidence angle versus radius are compared to the rotor requirements. The initial test data was acquired at 60% of design speed. Later measurements were carried out to speeds of 70% of design and the need to improve the inlet flow field at low speeds was clearly demonstrated, Ref. 2. It was found that the rotor inlet flow angle was, for a constant throttle setting, independent of speed. Attempts to improve the rotor flow were made by modifing the inlet. However, calculations as well as hardware modifications showed that the existing inlet flow (Fig. 2) could only be changed slightly by variations upstream of the rotor leading edge. In order to increase the flow rate, a flow straightener downstream of the stator was removed. This flow straightener (consisting of a honeycomb) was found to produce sizable losses and thus restrict the exit

flow. An increase in flow rate was measured, however, the velocity distribution at the rotor leading edge was not changed significantly. Consequently the role of the stator or the rotor-stator interaction was examined more thoroughly in order to understand the flow field measured in the compressor.

II. ROTOR - STATOR INTERACTION

Attempts to improve the rotor flow described in Ref. 2 dealt with the rotor inflow only. Since the rotor incidence angle was found to be constant, modifying the inflow using various hardware changes seemed to be a logical step. However, as the improvements achieved were small, the influence of the flow downstream of the rotor on the rotor itself became the center of attention. Tables I. through VI. show the radial distributions of rotor and stator and inlet angles. These measurements were taken as different inlet modifications were tried. (Ref. 2) The design speed was 60% at the indicated flow rates. In Fig. 3 the stator incidence angle is plotted versus the rotor incidence angle for five streamlines (also see Tables I through VI). Data for each of the radial surveys is connected with a curved line. For any of the given streamlines the relationship between stator and rotor incidence angle can be closely approximated by a straight line. This correlation was found to be independent of flow rate and radial distribution of flow rate at the rotor inlet. Certain distributions were forced by using various inlet screens (see Ref. 2). Consequently for any given rotor incidence angle there will only be one corresponding stator incidence angle. Close to the origin of the coordinate system (Fig. 3) a curved line indicates the relationship for minimum loss incidence angle of rotor and stator. The difference between the minimum loss incidence and any measured incidence indicates significant loss

production. From the straight lines (Fig.3) representing various streamlines, the necessary stator incidence angle corresponding to a minimum loss rotor incidence angle and vice versa can be determined across the blade span. Fig. 4 shows that a stator operating at minimum loss incidence angle would require the rotor to be stalled while a rotor minimum loss configuration would force the stator to surge. Any rotor inflow modifications can only bring about changes between these limits shown in Fig. 4.

While the rotor approaches minimum loss incidence angle with increasing flow rate, the stator improves with decreasing flow rate. Fig. 5 shows that at 60% of design speed the stator static pressure recovery increases with decreasing flow rate. To place the stator running conditions in the perspective of the overall compressor performance, the stator incidence angle at mid chord is compared to compressor efficiency (Fig. 6) at 70% of design speed. The compressor peak efficiency occurs at a flow rate quite close to the point where the stator is operating at minimum loss incidence angle. This indicated that the influence of the stator incidence on the compressor should be significant.

Although it was found that the rotor inflow was independent of wheel speed at 60% speed, it was important to determine if the relationship found between rotor and stator incidence conditions found at this speed would be the same at other speeds. For 70% of design speed the rotor and stator incidence angle distributions were measured at various flow rates. At 68% of design speed the rotor relative Mach number exceeds unity at the rotor tip. Beyond 60% the relative Mach number is already larger than the critical value. At these conditions the wake shed from a probe immediately upstream of the leading edge

(station 1, Fig. 1) can cause severe flutter problems for the rotor blading. To avoid damaging the machine a computer program was developed, which calculated the velocity vector at the rotor leading edge from measurements at measuring station number 0 (see Fig. 1). The incidence angle derived from this velocity vector differs only slightly from the value measured at station 1. For inlet configurations without any screens or other modifications the rotor and stator inlets were surveyed at 60 and 70% of design speed at the open and closed throttle settings. Tables VII through X show the results, which are plotted on Fig 7. Figure 7 shows that for a full open throttle configuration the curves of stator incidence versus rotor incidence are practically the same for either 60 or 70% of design speed. For throttled conditions there are slight differences, probably because the throttle setting was not exactly the same for both speeds. The data of all four curves can be represented by straight lines for individual streamlines. Only the flow rate changes with these curves. The compressor speed has no influence. In Fig. 8 the radial distributions of rotor and stator incidence angle are shown for two throttle settings at 70% of design speed. At the maximum flow rate (open throttle) the stator incidence is about -16° at the tip and negative over the whole blade span. For this running condition the rotor comes closest to the minimum loss incidence angle; the desired operating regime. However, the stator will be approaching surge and will generate a significant amount of blockage downstream of the rotor. Since it was clearly demonstrated that any improvement to the rotor flow would make things worse for the stator, the stator was removed.

III. COMPARISON OF ROTOR ONLY AND STAGE DATA

The stator was manufactured as a single piece rather than an assembly of a disk and blades (see Fig. 1). In order not to disturb the flow at the hub, the stator was replaced by an aluminum ring with a contour identical to the stator hub. This ring contained the same static pressure tappings as the original stator hub. The flow straightener (honeycomb) shown in Fig. 1 had been removed earlier. Thus the swirl created in the flow by the rotor was not removed. After the flow leaves the compressor stage (former end of flow straightener), it is turned 90° and exhausted radially. Within the exhaust, there were eight struts made of 0.75 inch diameter bolts with fairings. The area ratio between exhaust cross-section and rotor outlet is 0.82. Due to a corresponding reduction in axial velocity, the swirl angle in the exhaust is between 10° and 15°, depending upon spanwise location. Since the struts could not be adjusted to this angle, they were left misaligned to the flow by that amount. The misalignment was considered to be small since the struts occupied only 9.5% of the total exhaust area.

The total pressure/temperature probes of the stage outlet rake at measuring station number 3 were adjusted to the flow angle determined with an angle probe. For the flow rate range examined, the instrumentation did not need to be adjusted further. The removal of the stator required the disassembly of most of the test vehicle. Earlier tests had shown it to be an improvement to modify the rotor spinner to a strictly conical shape (Ref. 2). This disassembly was used to alter the existing spinner to the shape shown in Fig. 9. due to the forward extension beyond the original spinner tip, the traversing distance of the combination pneumatic/temperature probe at station 0 had to be reduced. Otherwise no further modifications of the

instrumentation hardware or software were necessary.

III.1. Overall Performance

Since it was found that the rotor operates closest to minimum loss incidence at full open throttle, the compressor map was not measured. For speeds from 25% to 70% the performance was measured at small increments of speed at open throttle. This data and performance map data of the stage acquired earlier is shown in tables XI to XIV. Fig 10 shows an appropriate comparison. For the stage configuration the speed lines of 60% and 70% of design speed are shown as well as the maximum flow rate line for speeds from 25% to 70%. The latter can be directly compared to the maximum flow rate line for the rotor only configuration. This shows that the total pressure rise produced by the rotor alone is slightly lower than the stage at the same speed, however the referred flow rate is higher. At the same time the overall efficiency is higher for the rotor only configuration. The total temperature increase is smaller for the rotor only (Fig. 11), which appears to be the primary reason for the increase in efficency. For any given speed the referred flow rate of the rotor alone is larger than the stage flow rate. This indicated, that the stator in fact generated increased downstream blockage at open throttle.

III. 2. Rotor In- and Outflow

The goal of removing the stator was to improve the rotor flow. Consequently the rotor in- and outflow were measured and compared with the stage data. Radial surveys were taken at measuring stations 0 (upstream) and station 2 (downstream of the rotor) (Fig. 1). Fig. 12a shows the absolute Mach number distribution. Although an overall increase in flow rate was measured, the increase in inlet Mach number shown is misleading. The

change of the spinner increased the hub radius at station 0. This represented an area reduction at that axial location of 3.3%, which partially led to the increase in Mach number shown. At the rotor outlet (station 2) the radial distribution of the absolute Mach number did not vary, while the level dropped slightly. The absolute flow angle (Fig. 12b) shows basically no change between stage and the rotor only measurement. At station 0 there was a small deviation in absolute angle near the hub for the rotor only configuration. This cannot be attributed to preswirl due to the changed spinner geometry, since preswirl would produce a flow deflection in the opposite direction. It had to be assumed that there was a measurement error. Changes at measuring station 2 were small. The disagreement with the design values did not improve. The flow pitch angles at stations 0 and 2 are shown in Fig. 12c. At the inlet (station 0) the pitch angle was slightly larger in a stage configuration than for the rotor only. Near the hub spinner, pitch angle is higher in the rotor only measurement while the pitch angle decreases towards 0° (the free stream value) for the stage configuration. No significant variations were found in the rotor outlet pitch angle distribution.

From the measured rotor inlet velocity vector and the rotational speed one can derive the incidence angle to the rotor. In Fig. 13, the rotor incidence angle for the rotor alone and the stage are compared. Due to the increased flow rate the rotor only configuration has lower incidence angles across the blade span. For a substantial center portion the measured incidence angle closely matches the value for minimum loss.

The hub to tip distribution of incidence angle did not change with the removal of the stator.

IV. ROTOR ONLY COMPARISON OF TEST RESULTS AND CALCULATIONS

For an open throttle, highest flow rate configuration, the radial distributions of velocity vector at rotor in - and outlet were measured at 70% of design speed (Fig. 14a-c). Qualitatively the distributions of absolute Mach number, yaw and pitch angle are the same as those for 60%, only the level of Mach number is increased. In order to have some means to derive total pressure losses across the rotor, the radial distributions of total pressure and temperature were measured at rotor in- and outlet (Fig. 15a, 15b). While the total temperature rise is fairly uniform across the blade span, the total pressure increase for the tip is small compared to the hub. These trends are reflected in the total pressure loss coefficient (Fig. 15c).

To evaluate the measurements further, a 2-D finite element computer code was used to calculate the rotor flow for the same running conditions. The code utilized was developed by Hirsch and is described in Ref. 3 and Ref. 4. The meridional mesh used in the calculation is shown in Fig. 16. The station lines (hub to tip) are arranged such that line number 3 originates at the spinner tip, number 5 and number 8 coincide with the measuring stations number 0 and 1 respectively for radial surveys of the inlet. Number 9 represents the rotor leading edge and number 12 the trailing edge. Station line number 13 is identical to measuring station number 2, for radial surveys of the rotor outlet. The up- and downstream extensions of the mesh reach points where the duct cross-sectional areas remain constant. Inlet conditions such as flow rate, rotor speed, pressures and temperatures were taken from measurements at 70% of design speed. The results given by the computer code are very extensive and only a few are presented. The calculated flow angle (Fig. 17) is in good agreement with the measurement for rotor in-and outflow.

Disagreement towards the tip at measuring station 2, calculation station 13 is likely to be a probe error. The probe is retracted into a 0.25" diameter hole, leaving a gap between the probe itself and the outside of the hole. Furthermore, not all sensors are located at the same radial position, so that some might already be retracted while others are still exposed to the flow. The combination of these effects causes inaccuracies in measurements in the immediate vicinity of the wall. In Fig. 18 the velocity in the absolute frame is compared for various axial stations. The agreement is good everywhere. Test data plotted at calculating station number 9 has been calculated from measurements at measurement station number 0. In order to evaluate the whole velocity vector, the various components of the absolute total velocity (Fig. 18) were compared. While the agreement of the axial component is good throughout (Fig. 19), large discrepancies appear to exist for the radial component of the rotor outlet. Here, however, the representation of the three dimensional velocity vector in terms of its components rather than magnitude and angles, is misleading. In fact, if one neglects discrepancies in the tip region, the largest difference in radial velocity component of about 12 m/s at 32% blade span, represents an error in pitch angle of 3° less than everywhere else. Although not a negligible difference, an explanation was not readily available. For measuring station number 0/calculation station number 5, the error in pitch angle in the hub area is rather large. The maximum difference between 12° measured and 21° calculated at 20% span can only be accounted for by the substantial area change at calculation station number 3; this might have caused a problem in the calculation. The tangential velocity component (Fig. 21) is in good agreement for the lower 80% of the span at the rotor outlet. The disagreement in the upper 20% cannot be

attributed to probe error alone, since these only occur within 10% from the casewall. At 75% span the calculated absolute velocity shows only a small increase, while the absolute flow angle increases for that location. This could be the reason that the tangential velocity component increases. From the measured absolute flow angle (Fig. 17) and velocity (Fig. 18), the relative flow angle at rotor in-and outlet were calculated and compared to those derived from the throughflow calculation (Fig. 22). Except for the hub and tip area the agreement is good. Another parameter that was important in the calculation of profile losses is the relative Mach number. It was derived hub-to-tip for in-and outlet from measurements and compared to calculation results (Fig. 23). The agreement at the rotor leading edge is very good. For the outer 50% of the blade span the Mach number is larger than the critical value and reaches unity at the tip of the blade. The largest discrepancy in the outlet relative Mach number is 5% near the hub (Fig. 23). The measured qualitative behavior, however, is well predicted.

The combination probes resolve not only the velocity vector, but total pressure and total temperature as well. These quantities are needed to calculate the rotor losses. The inlet conditions are identical for measurement and calculation, due the measured data being used as the input for the calculation. Fig. 24 shows the total pressure at rotor in- and outlet. The measured increase in total pressure across the rotor is up to 12% less than the calculated one. In the tip region the discrepancy is rather large. Here the discontinuity in the calculation results noted earlier might be at fault.

In comparing the outlet total temperature (Fig. 25), one notes that the measured data points are scattered about the calculated values. The mass

averaged value of all single measurements however is close to the average value of the calculation. In earlier measurements it was found, that the temperature of the ambient air fluctuates as much as 2°C within short time periods. To avoid an influence of this phenomena on compressor measurements, the temperature differential across the rotor is measured rather than the absolute readings of in-and outlet. This procedure makes the temperature level of the incoming air unimportant. In Fig. 25 however, the actual values of the measured outlet total temperature are compared. They exhibit the magnitude of possible variations due to changes in ambient conditions. From the measured total pressures and total temperatures the rotor loss (hub to tip) was calculated (Fig. 26). The comparison with calculation results reflects the disagreement found in the total pressure (Fig. 24). Calculation as well as measurement show a distinct increase in losses towards the tip (80% span and larger). This is assumed to reflect the shock losses, which should be present at those radii due to the high relative inlet Mach number (Fig. 23).

V. CONCLUSION

The interdependence of rotor and stator flow of a transonic compressor was investigated. Starting from the observation that neither blade row was operating close to minimum loss conditions for any compressor speed and flow rate, it was found that for a wide array of rotor inlet conditions the dependence between rotor and stator flow followed a very distinct pattern. Changes of radial distributions of the inflow, generated by partial blockage, did not affect the relationship between rotor and stator flow for given streamlines. Since the rotor's optimum flow condition required the stator to be off-design and vice versa, the stator was removed so that the rotor could

operate without downstream blockage generated by the stator. Interestingly, the increase in flow rate observed was slight and changes in the rotor flow were moderate.

The flow of the rotor itself was compared with the calculation of a finite element computer program. The program was found to closely predict the measured flow.

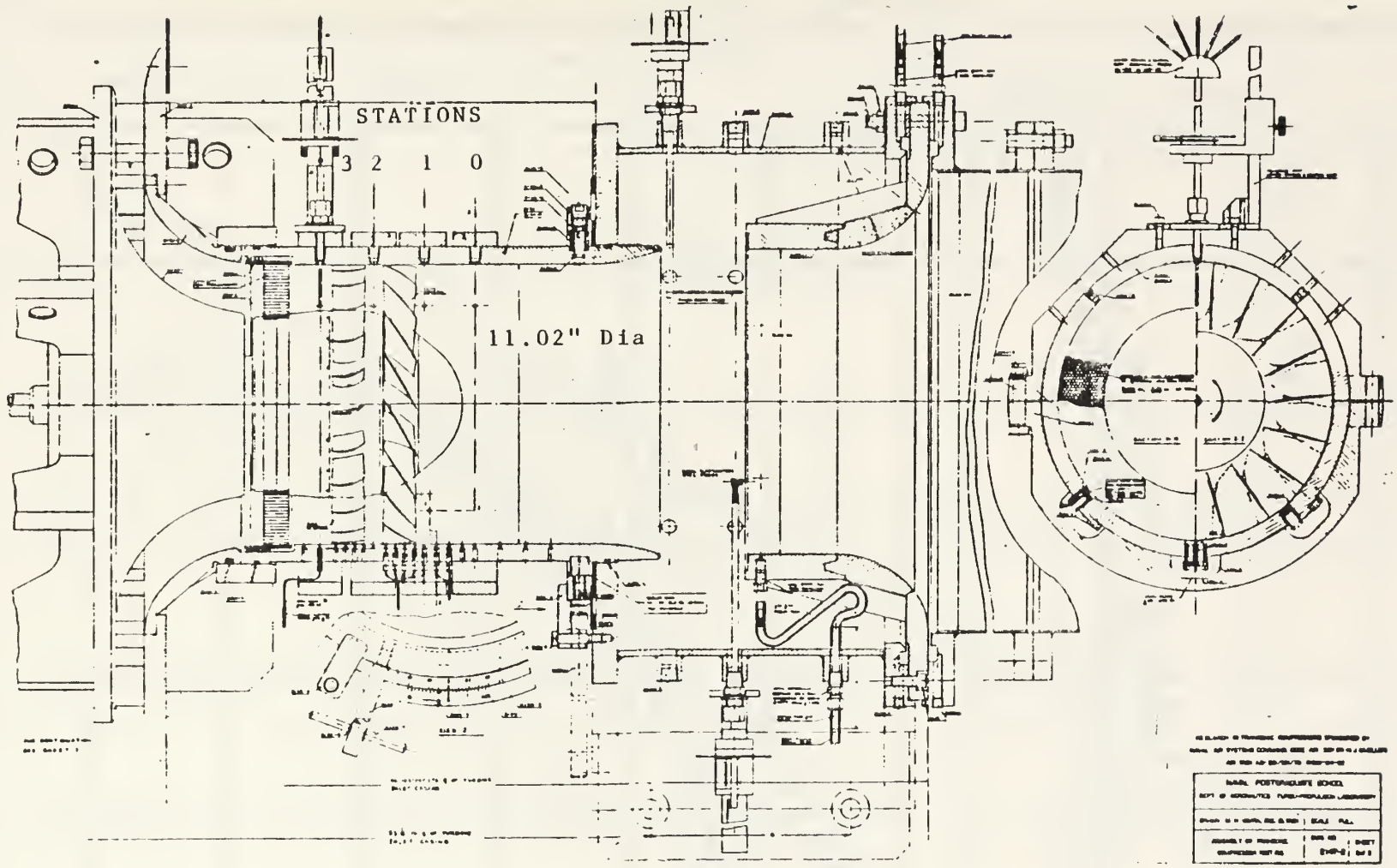

Figure 1. Transonic compressor.

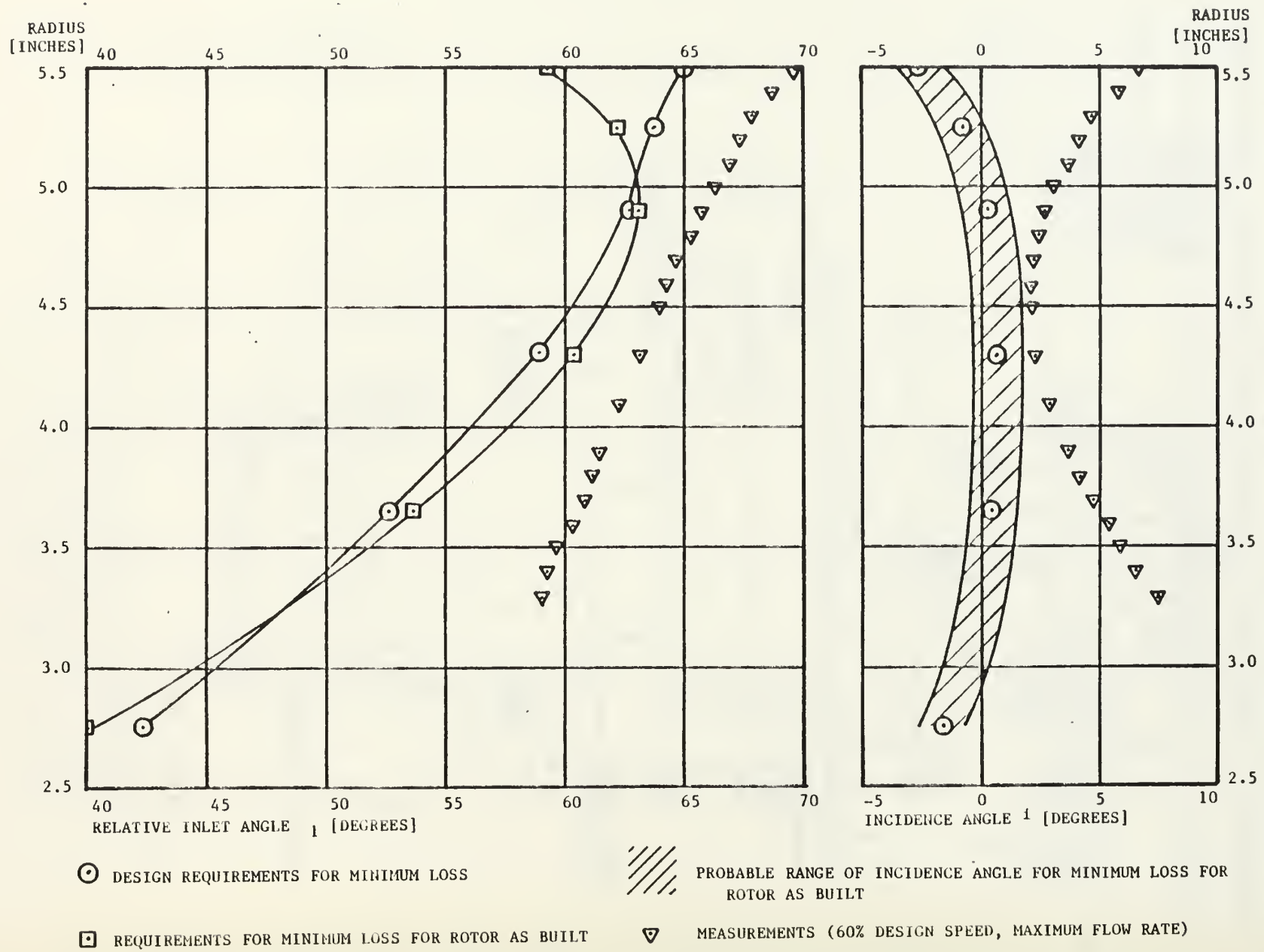

Figure 2. Radial distribution of relative rotor inlet angle (β_1) and rotor incidence angle (i) at 60% of design speed.

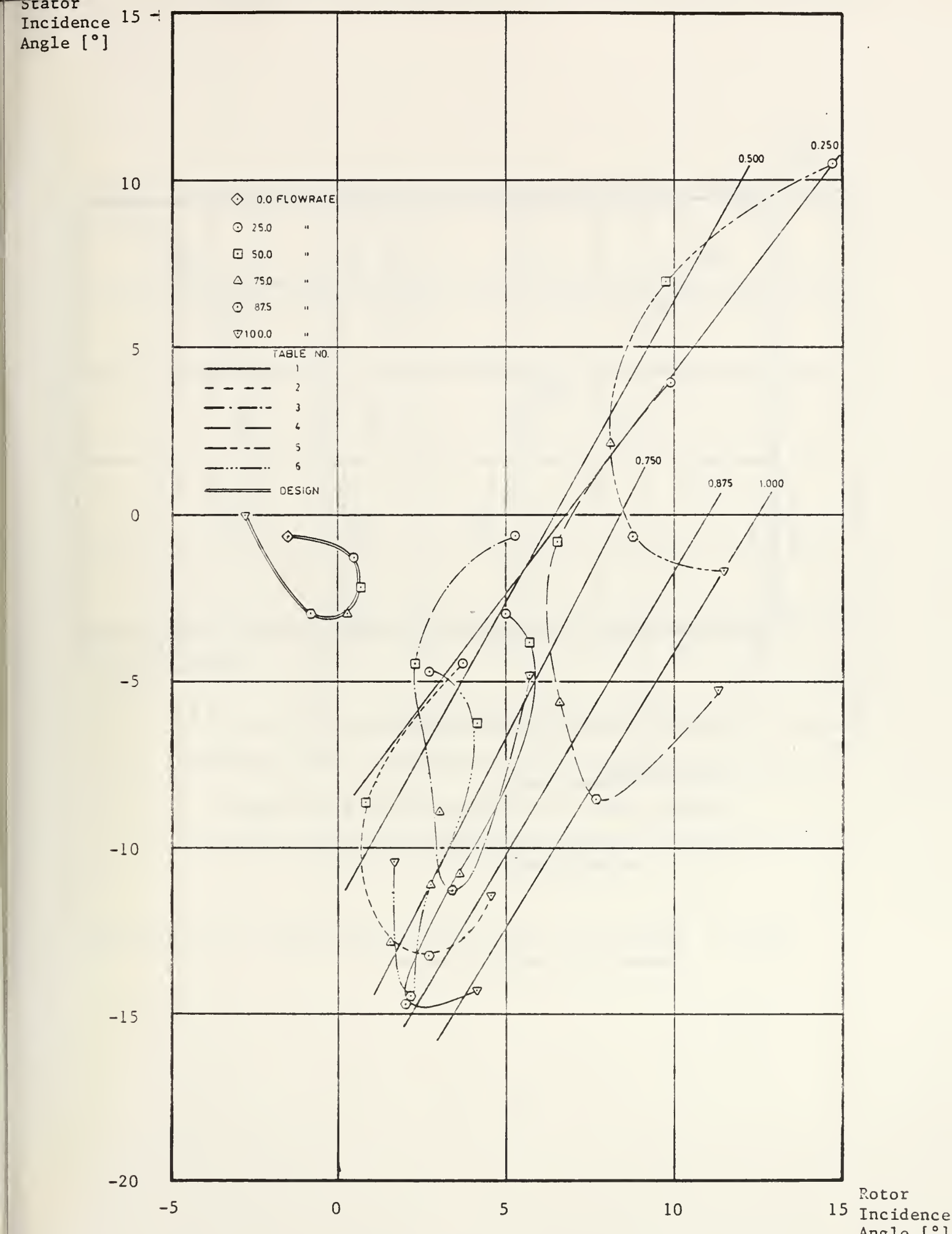

Figure 3. Stator incidence angle vs rotor incidence angle at 60% of design speed.

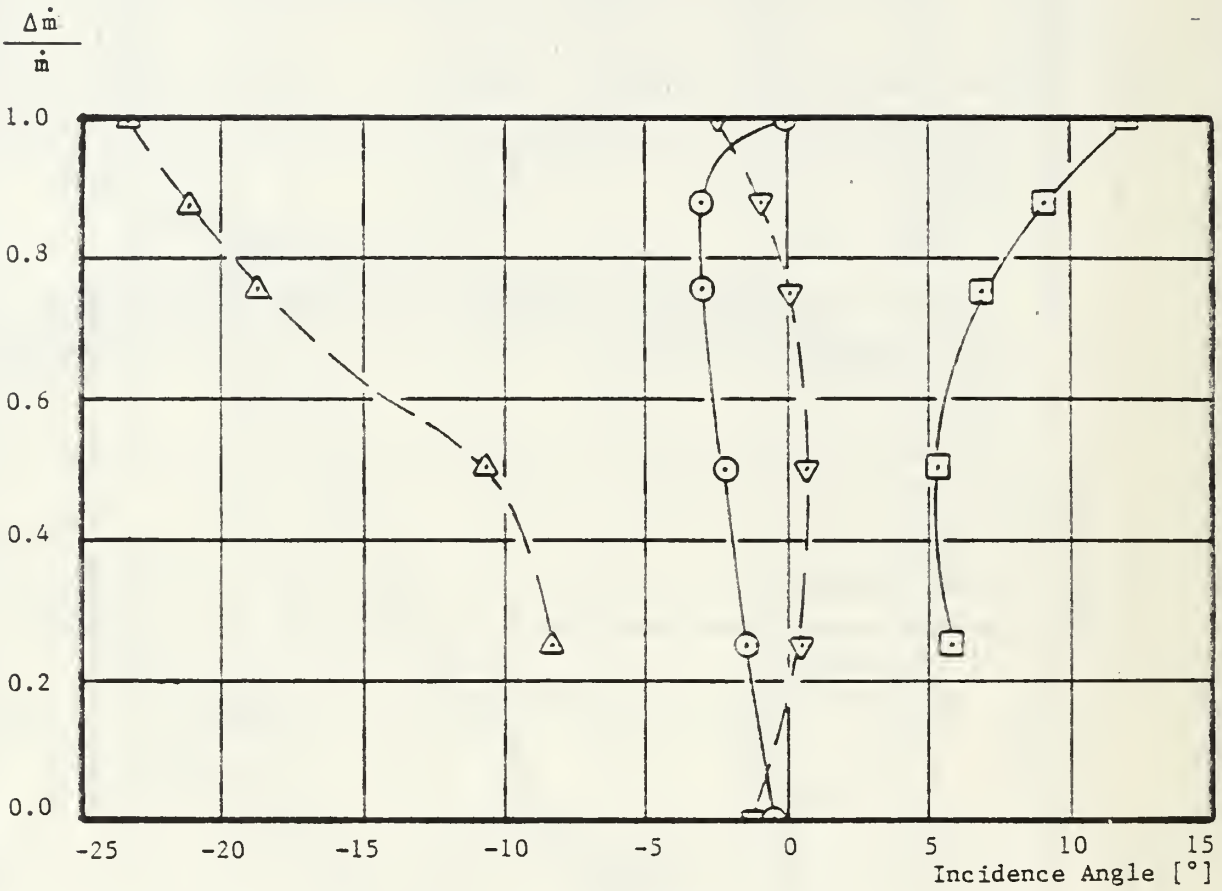

⊙ Stator minimum loss incidence angle

⊡ Rotor incidence angle corresponding to stator minimum loss incidence angle

▽ Rotor minimum loss incidence angle (original figures)

△ Stator incidence angle corresponding to rotor minimum loss incidence angle

Figure 4. Minimum loss rotor/stator incidence angle and corresponding stator/rotor incidence angle.

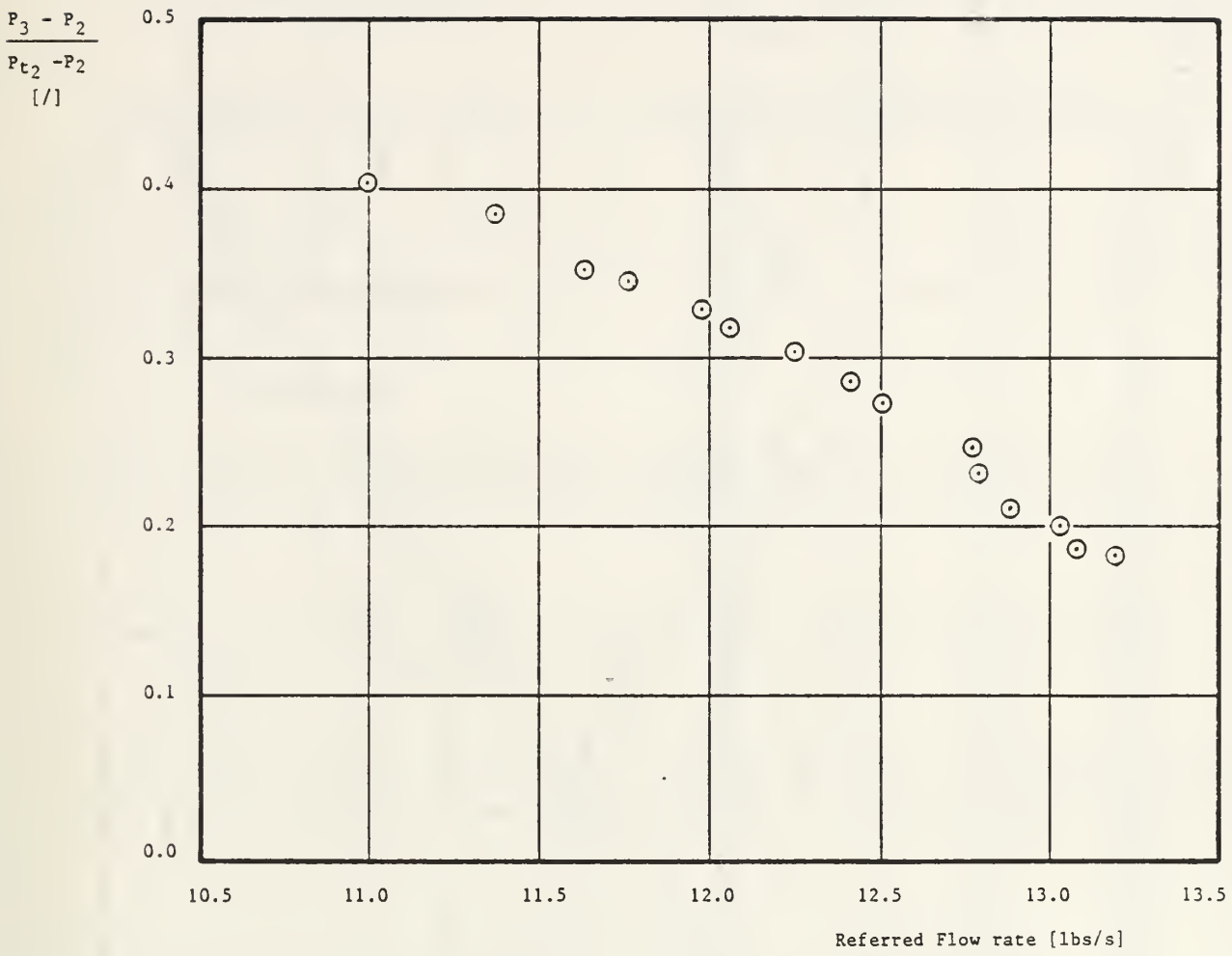

Figure 5. Stator static pressure recovery vs referred flow rate at 60% of design speed.

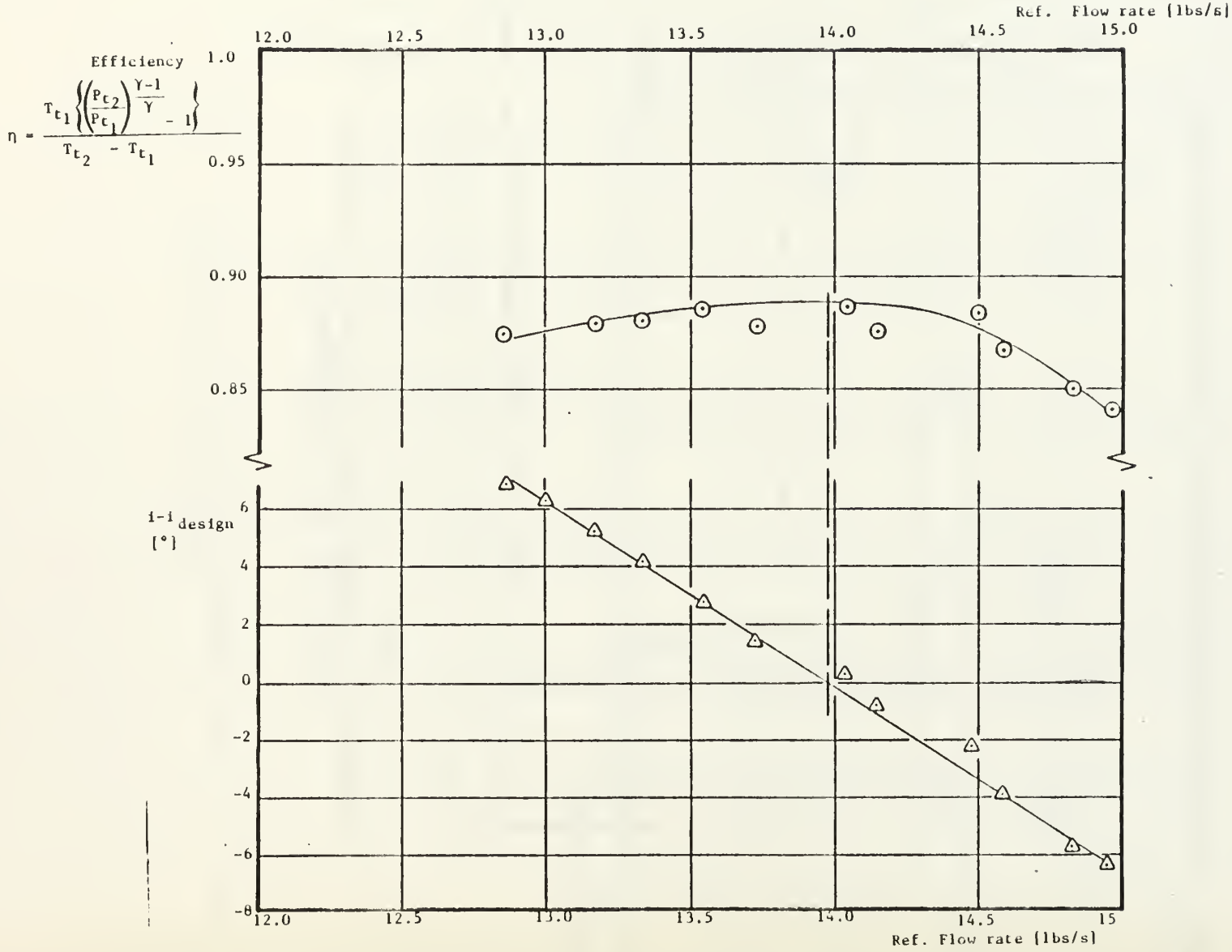

Figure 6. Stage efficiency and stator incidence angle deviation (i-i design) vs referred flow rate for 70% of design speed.

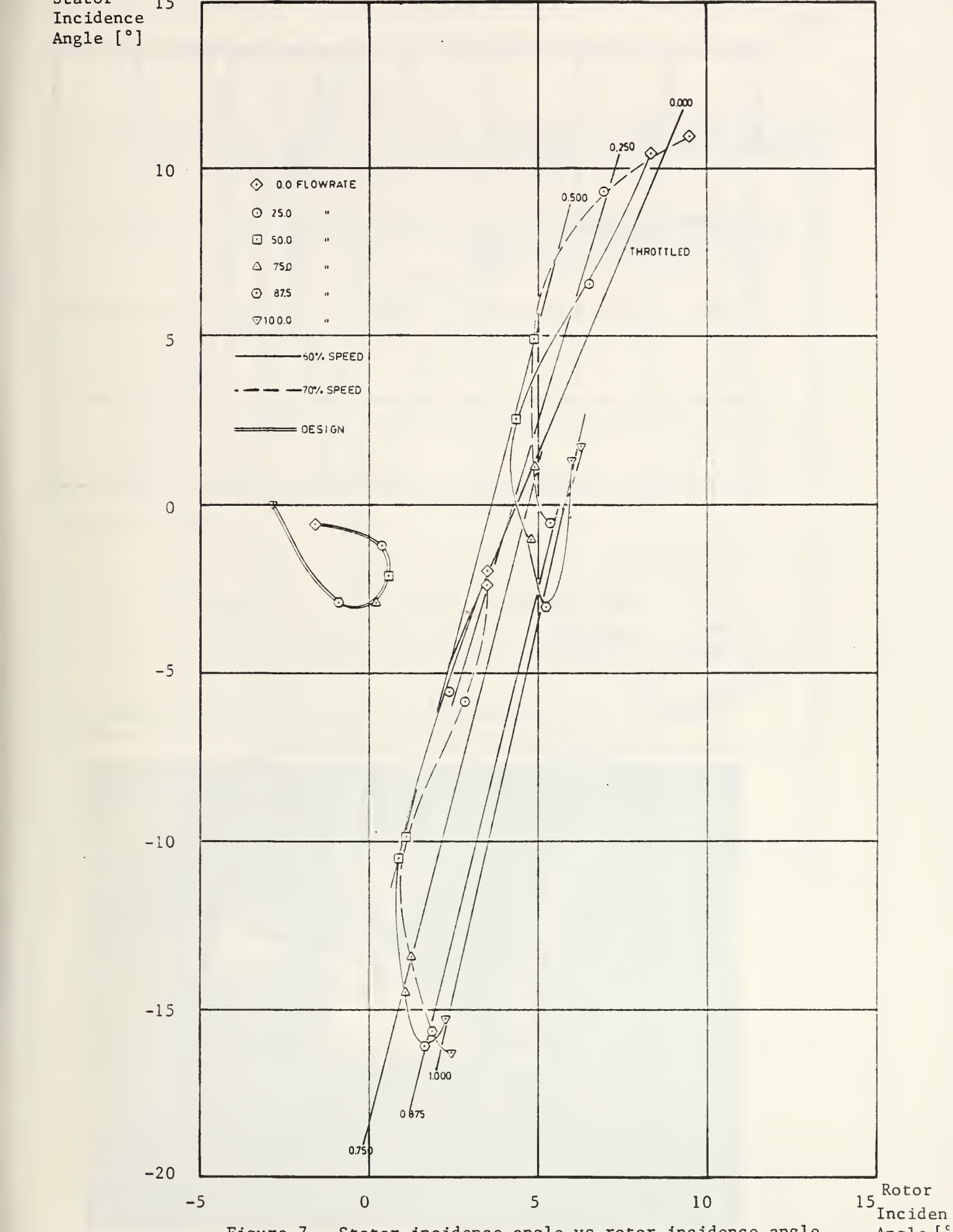

Figure 7. Stator incidence angle vs rotor incidence angle at 60% and 70% of design speed for two throttle conditions each.

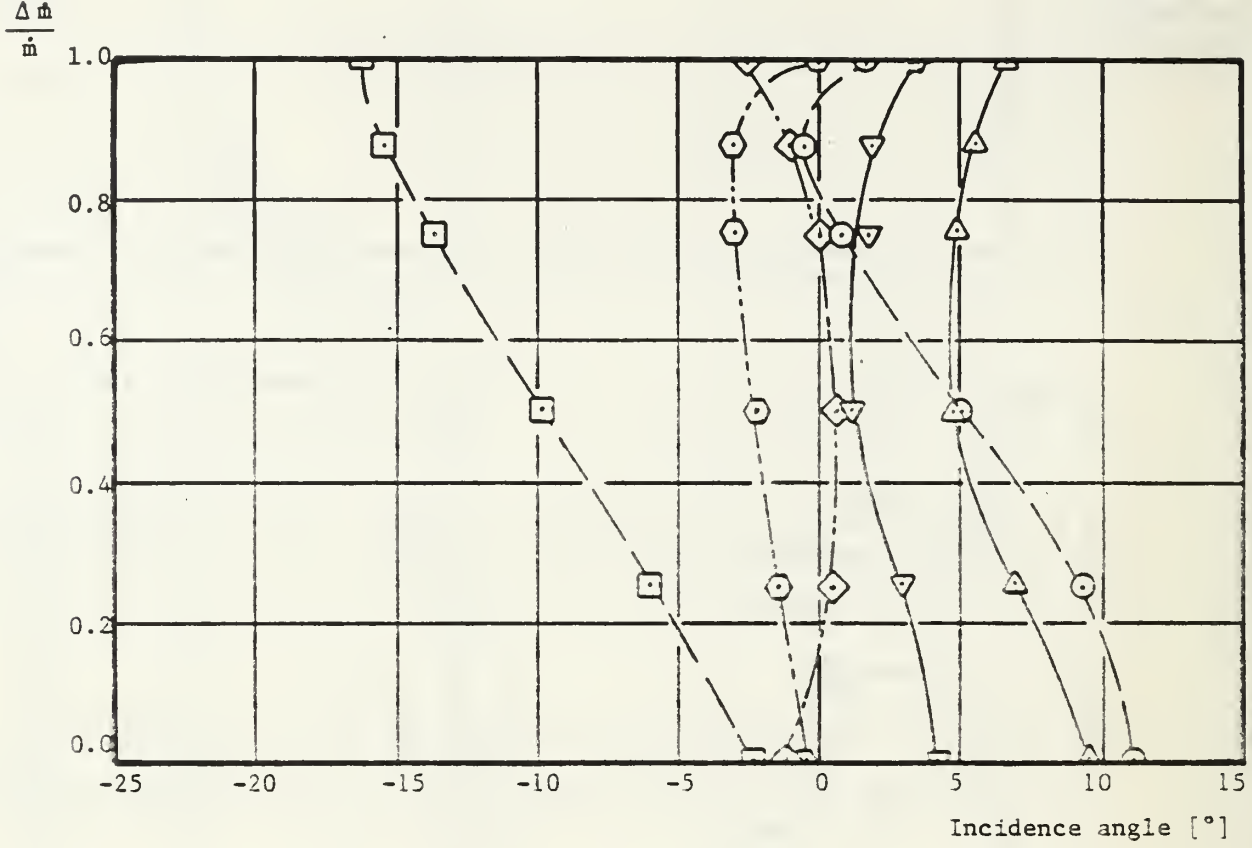

Figure 8. Radial distributions of rotor and stator incidence angle for various throttle settings at 70% of design speed.

Figure 9. Modified spinner.

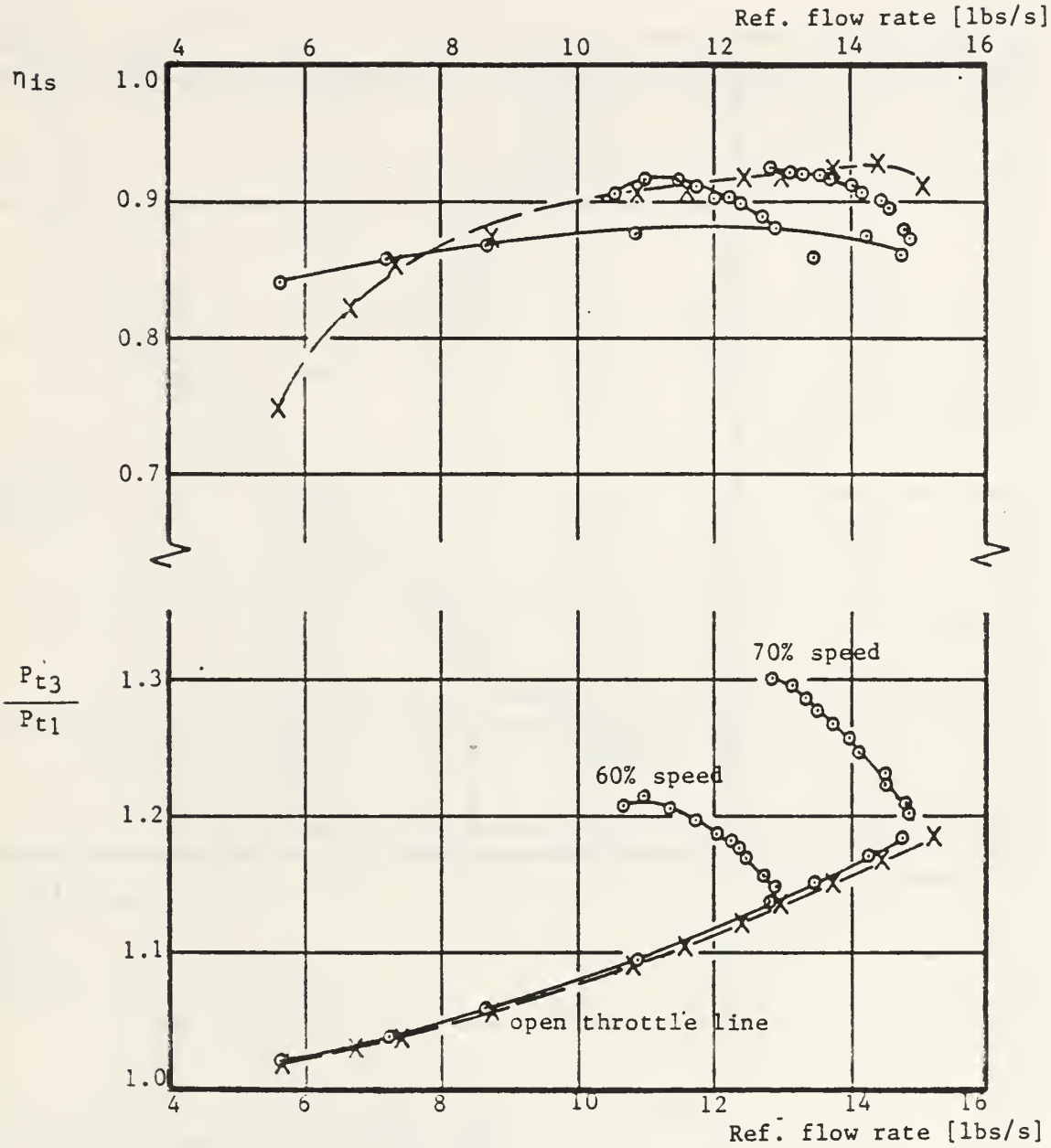

Figure 10. Compressor stage and rotor only performance map.

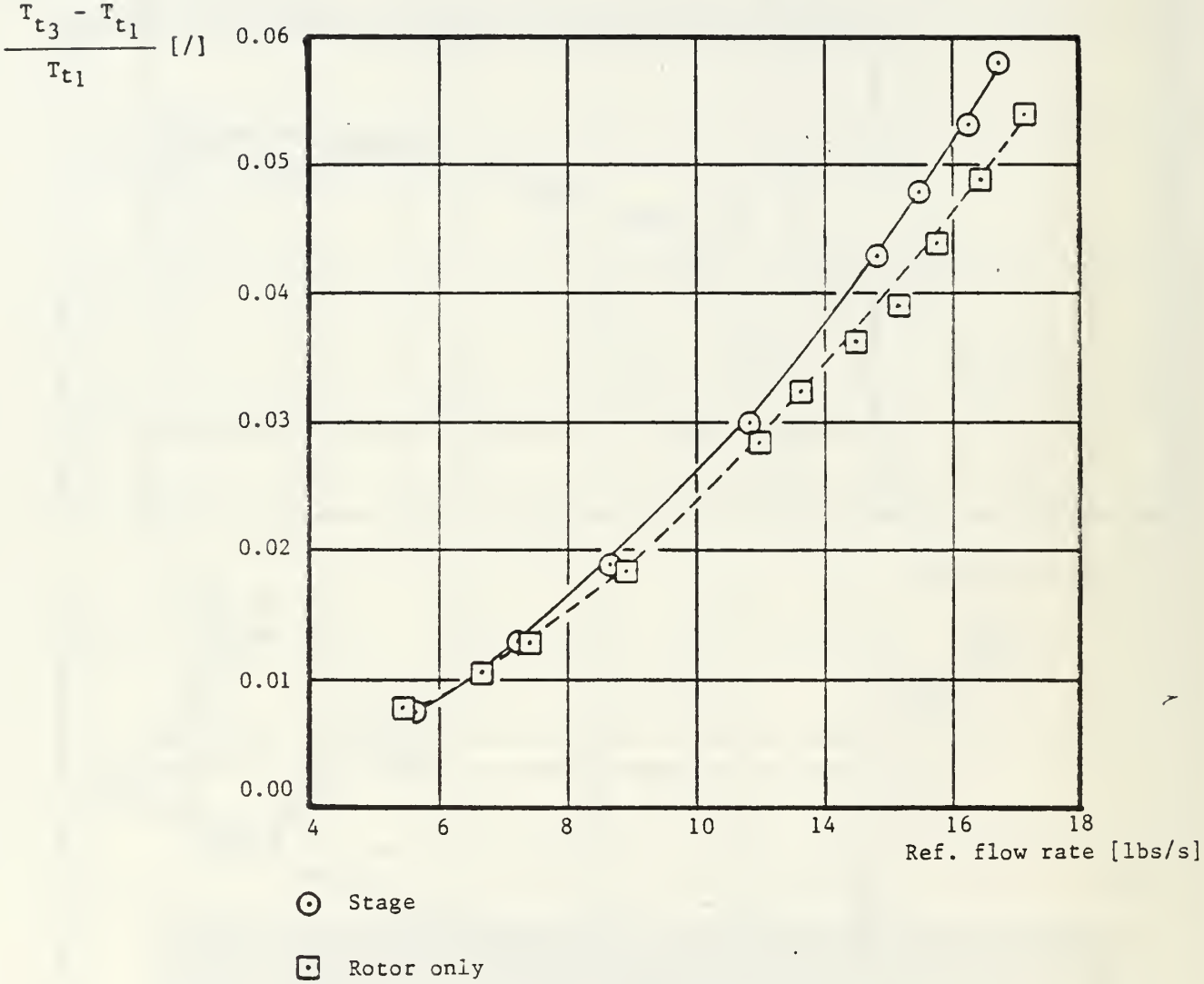

Figure 11. Open throttle (maximum referred flow rate) total temperature rise vs referred flow rate for compressor stage and rotor only.

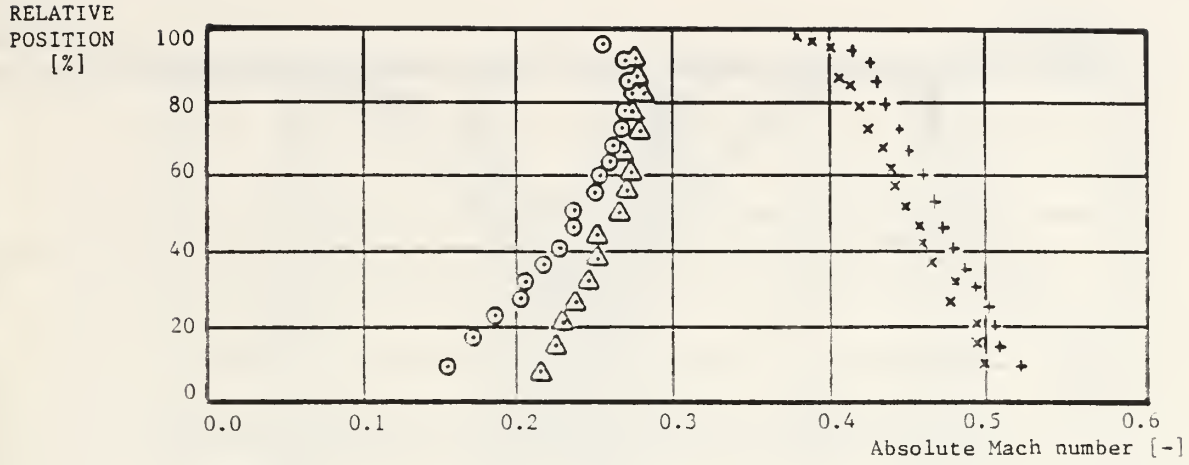

Fig. 12a

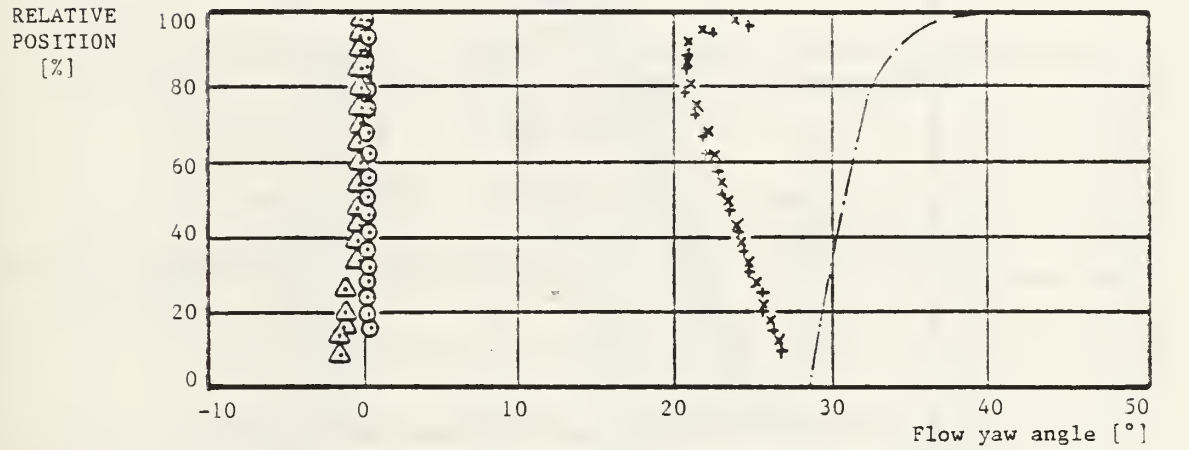

Fig 12b

(——·——·—— design values)

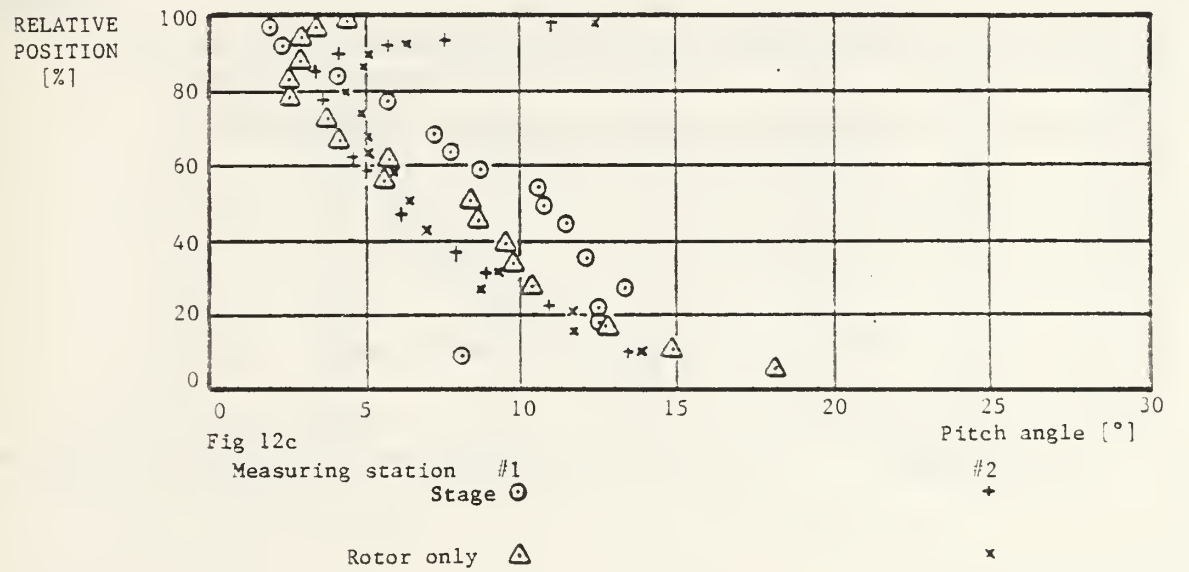

Fig 12c

Figure 12. Radial distributions of rotor in- and outlet velocity vector for stage and rotor only configuration at 60% off design speed.

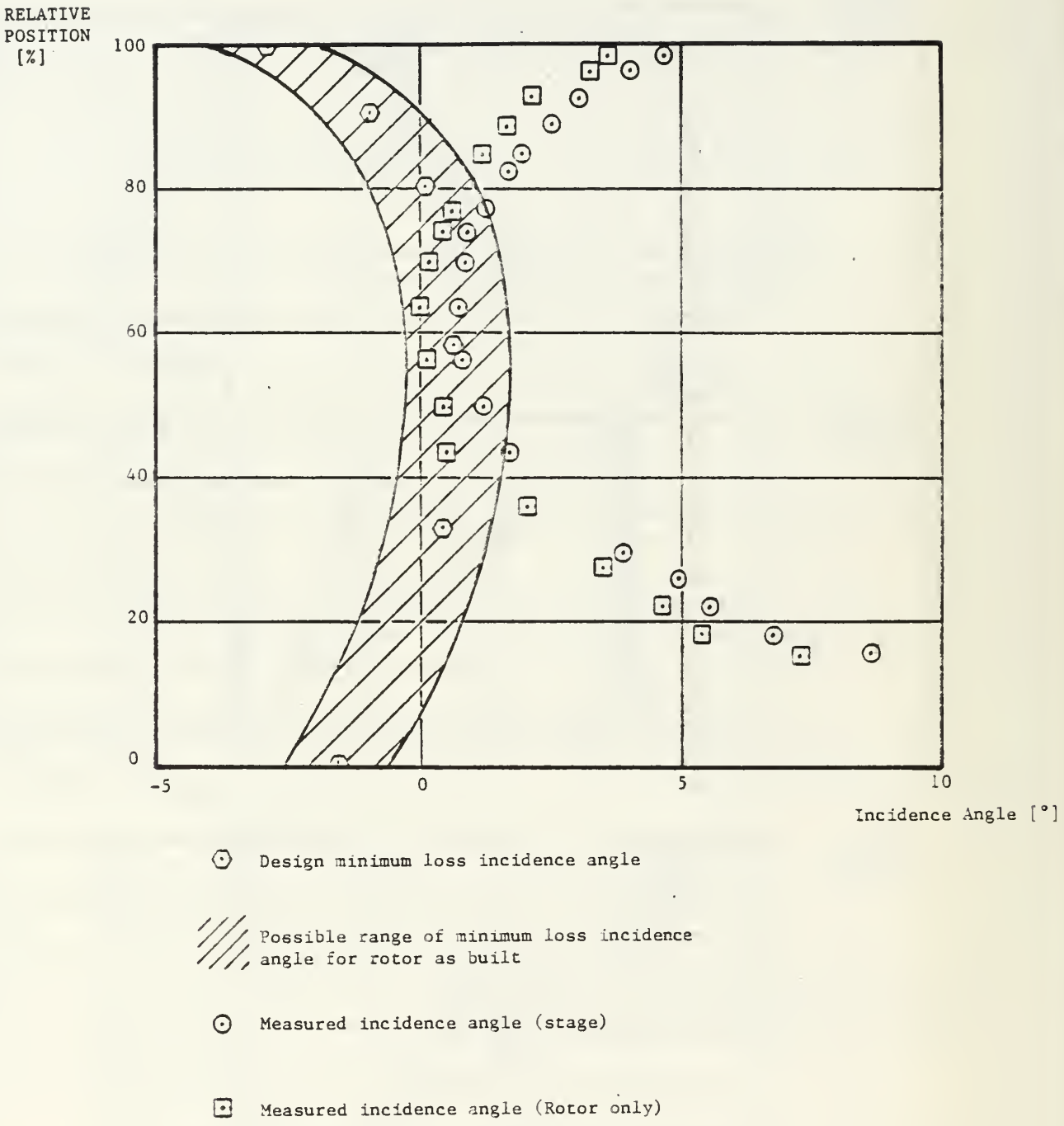

Figure 13. Rotor incidence angle vs blade span for stage and rotor only configuration.

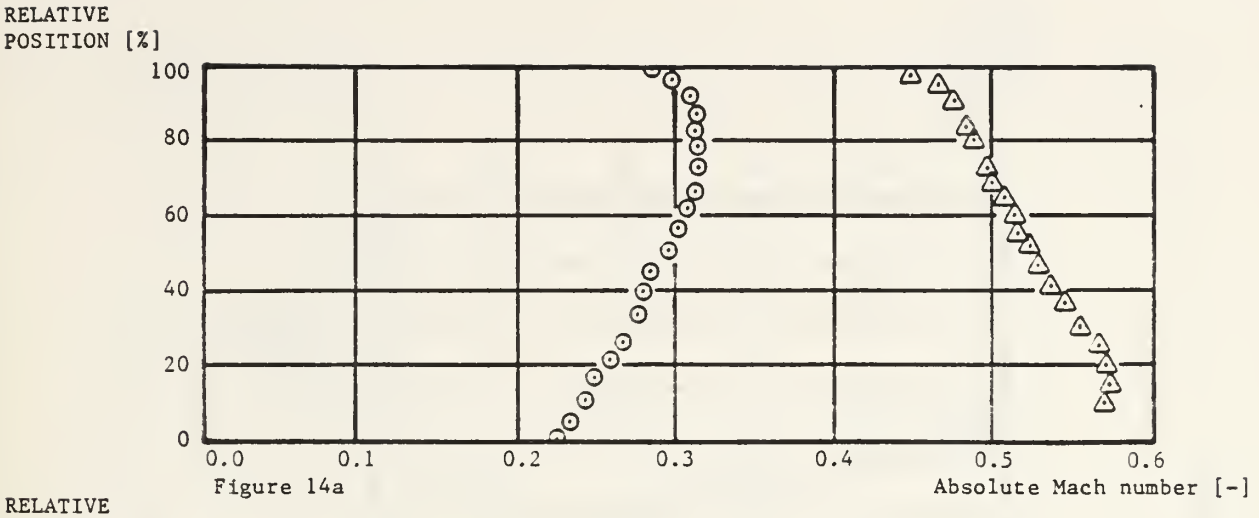

Figure 14a

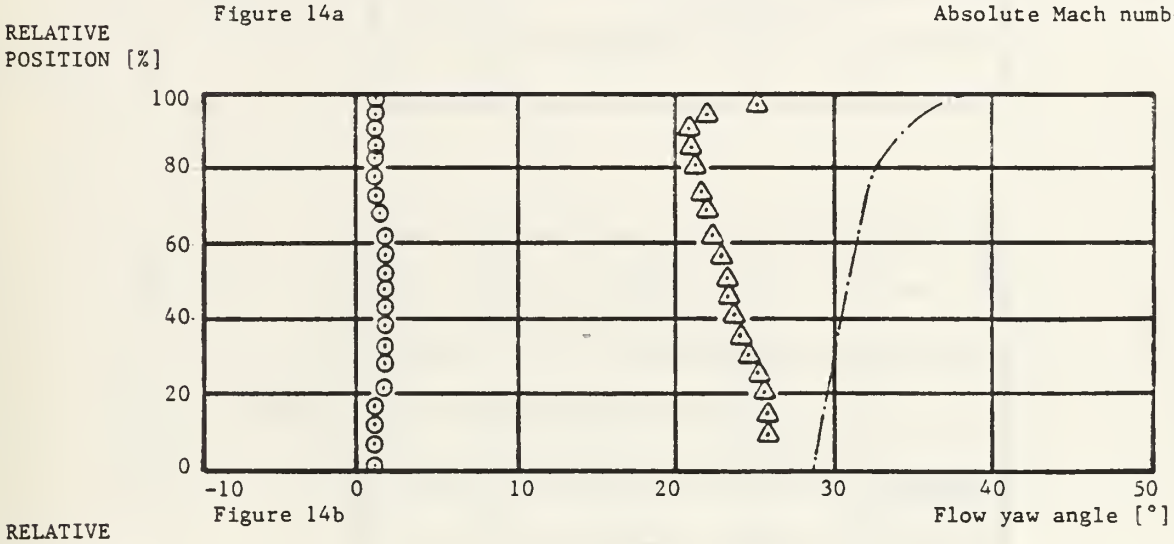

Figure 14b

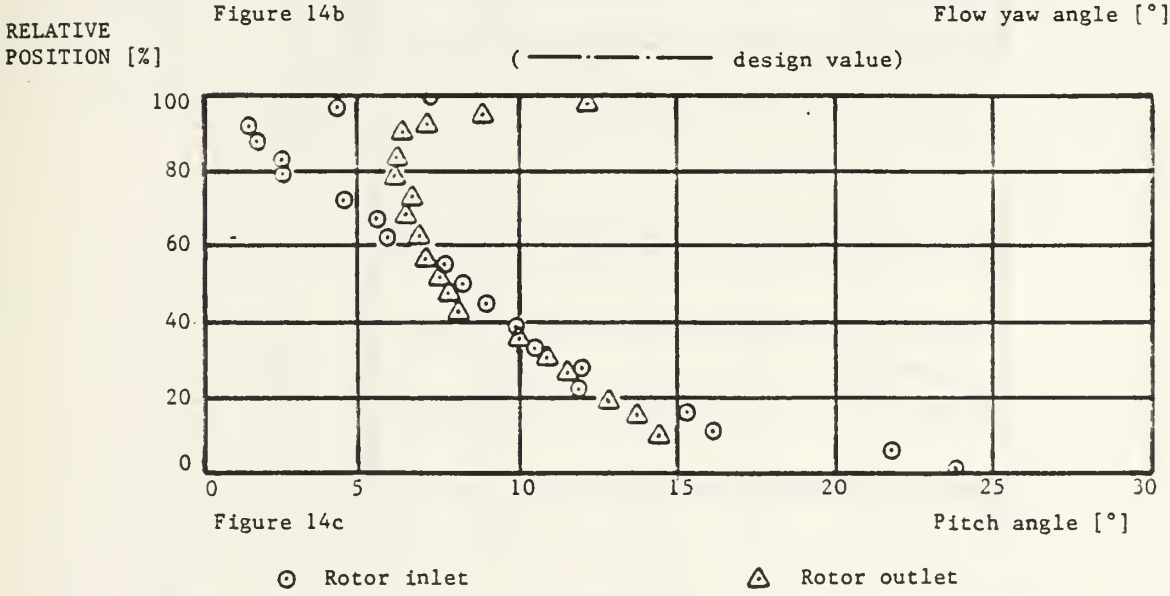

Figure 14c

Figure 14. Radial distributions of rotor in- and outlet velocity vector for rotor only configuration at 70% design speed.

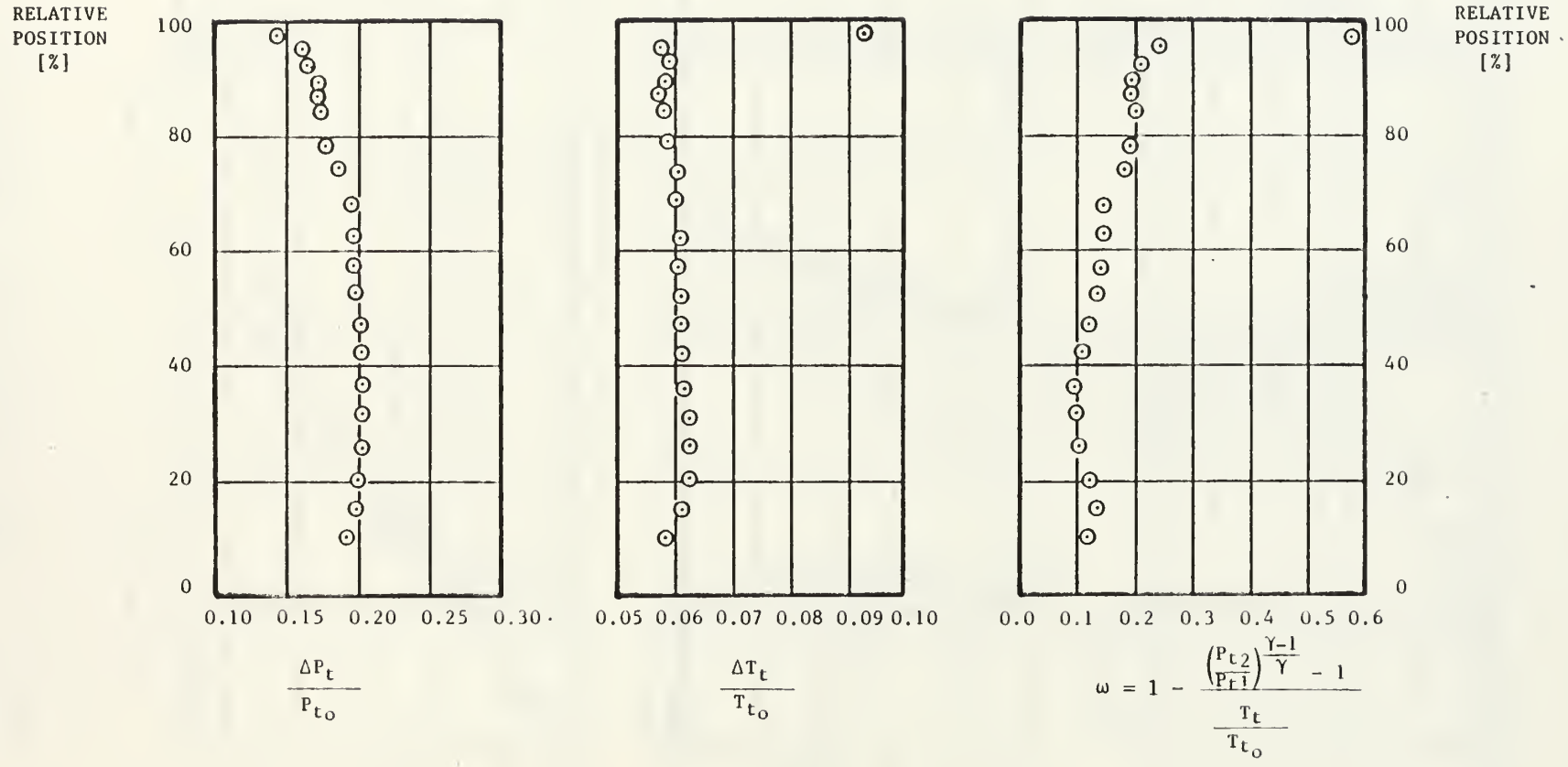

15a Total pressure rise

15b Total temperature rise

15c Loss

Figure 15. Radial distribution of rotor aero-thermodynamic measurements at 70% of design speed.

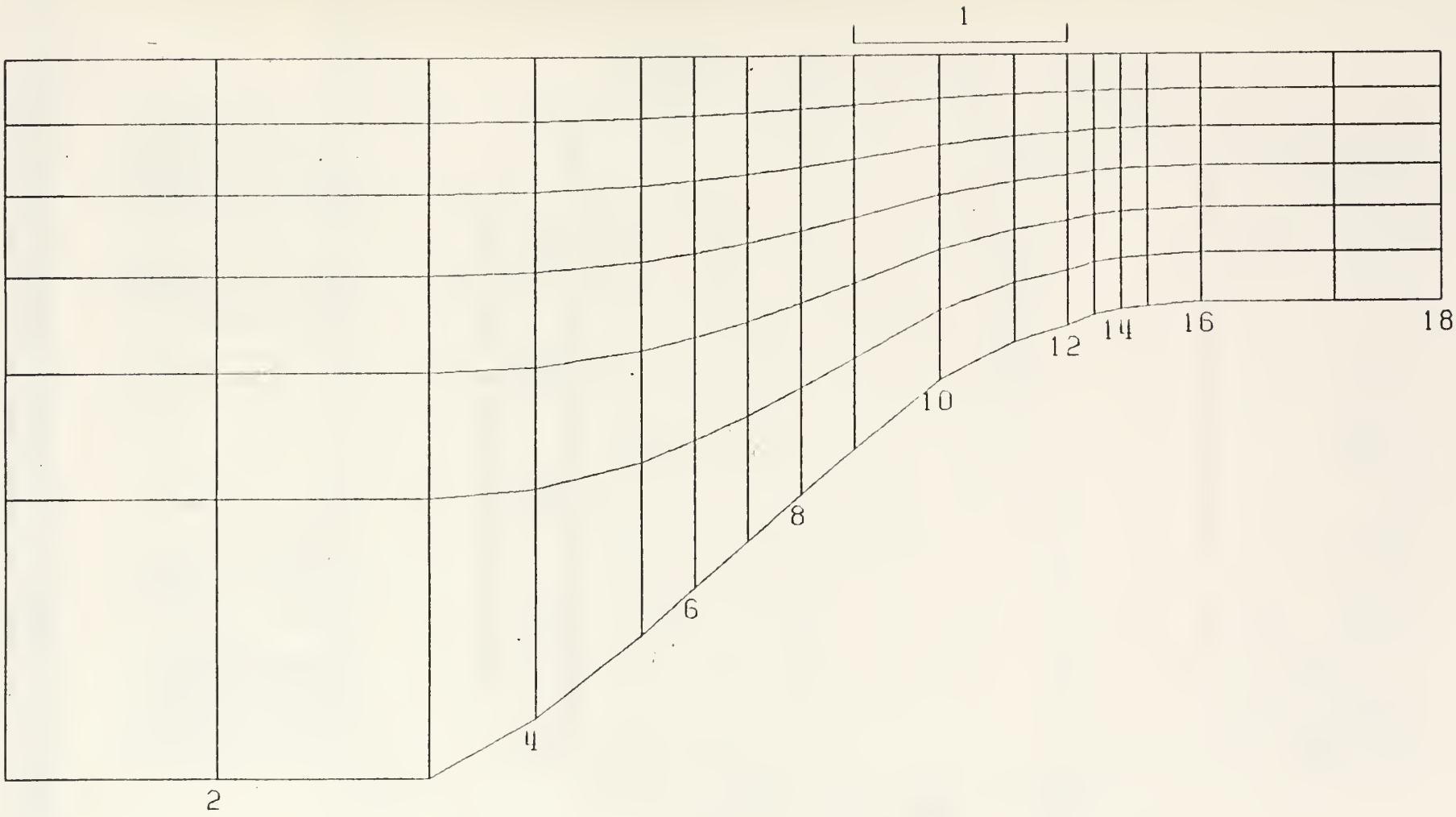

Figure 16. Computational grid of finite element program TURBOFEM.

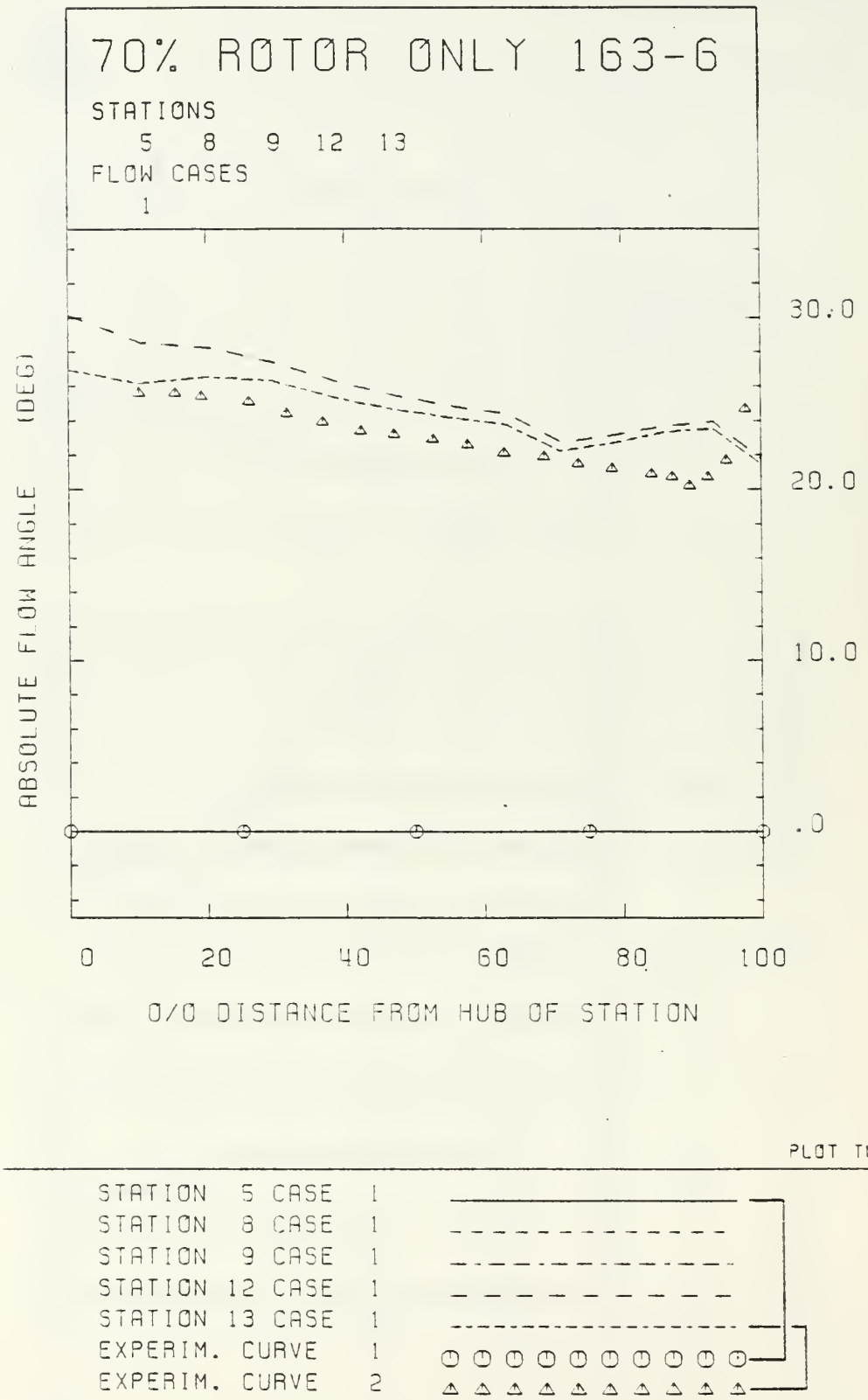

Figure 17. Comparison of measured and calculated absolute flow angle vs blade span at 70% of design speed.

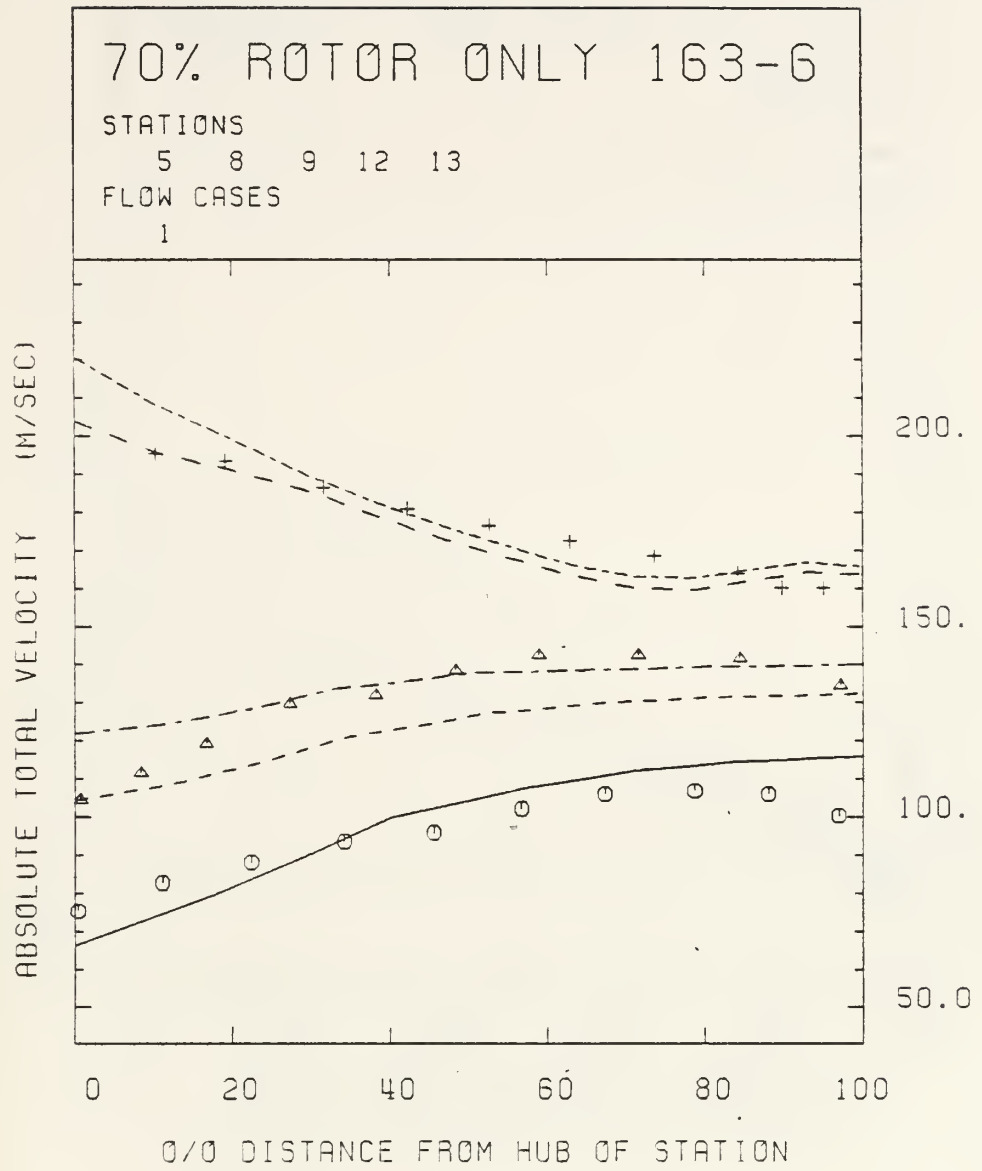

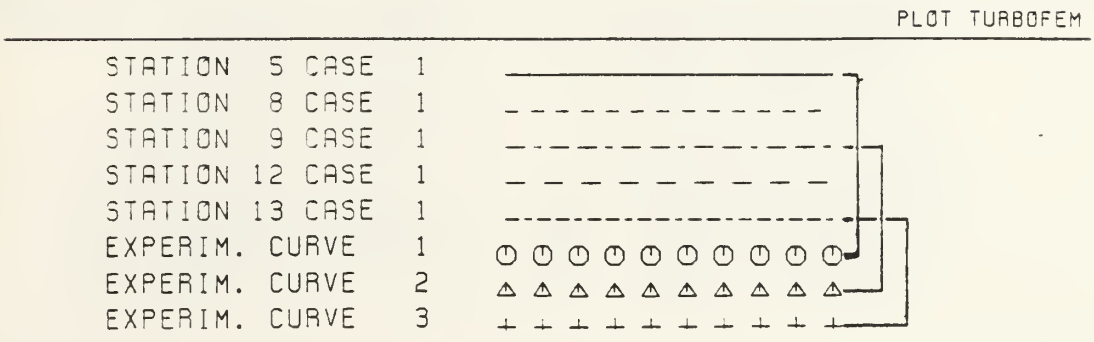

Figure 18. Comparison of measured and calculated absolute total velocity vs blade span at 70% of design speed.

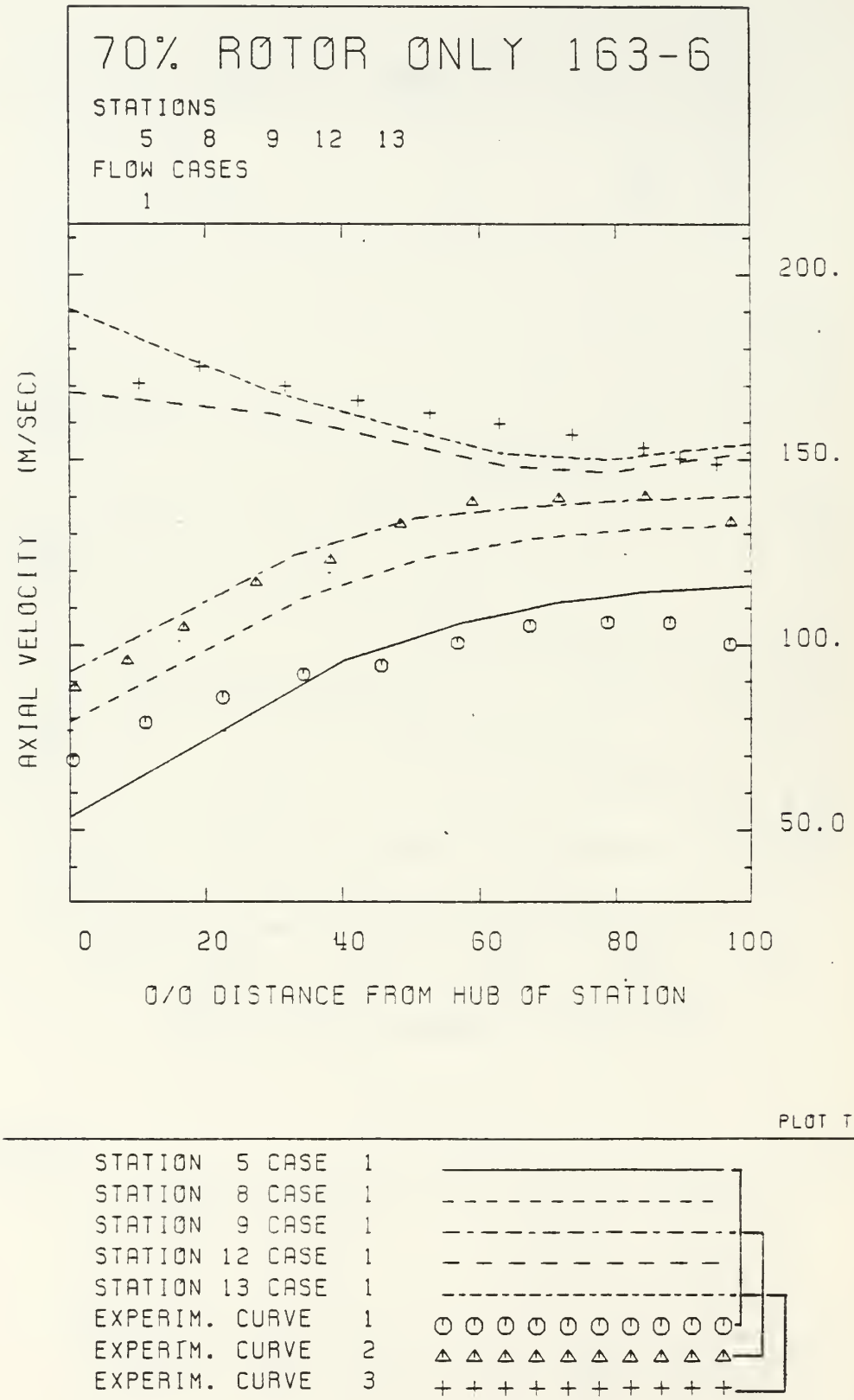

Figure 19. Comparison of measured and calculated axial velocity component vs blade span at 70% of design speed.

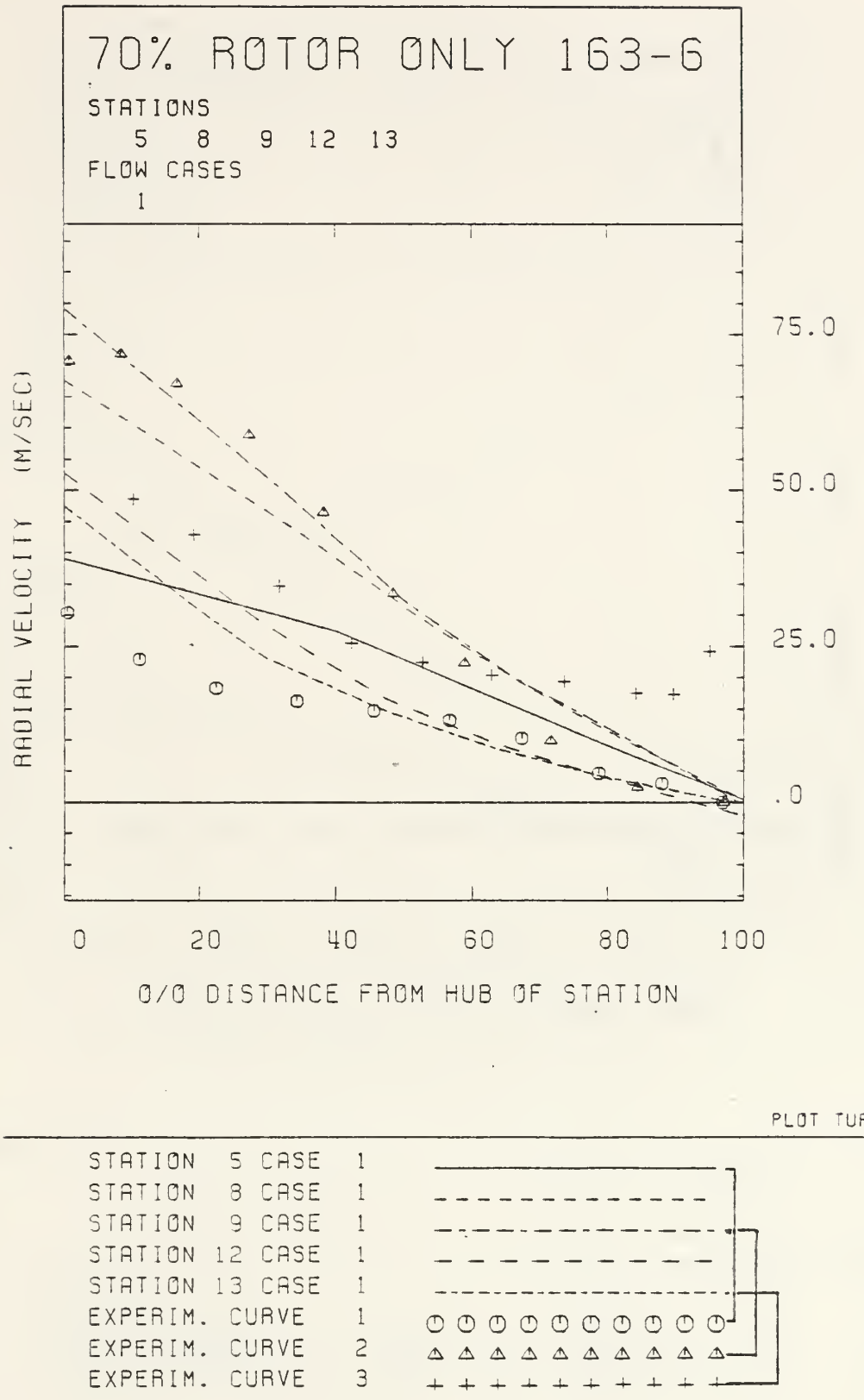

Figure 20. Comparison of measured and calculated radial velocity component vs blade span at 70% of design speed.

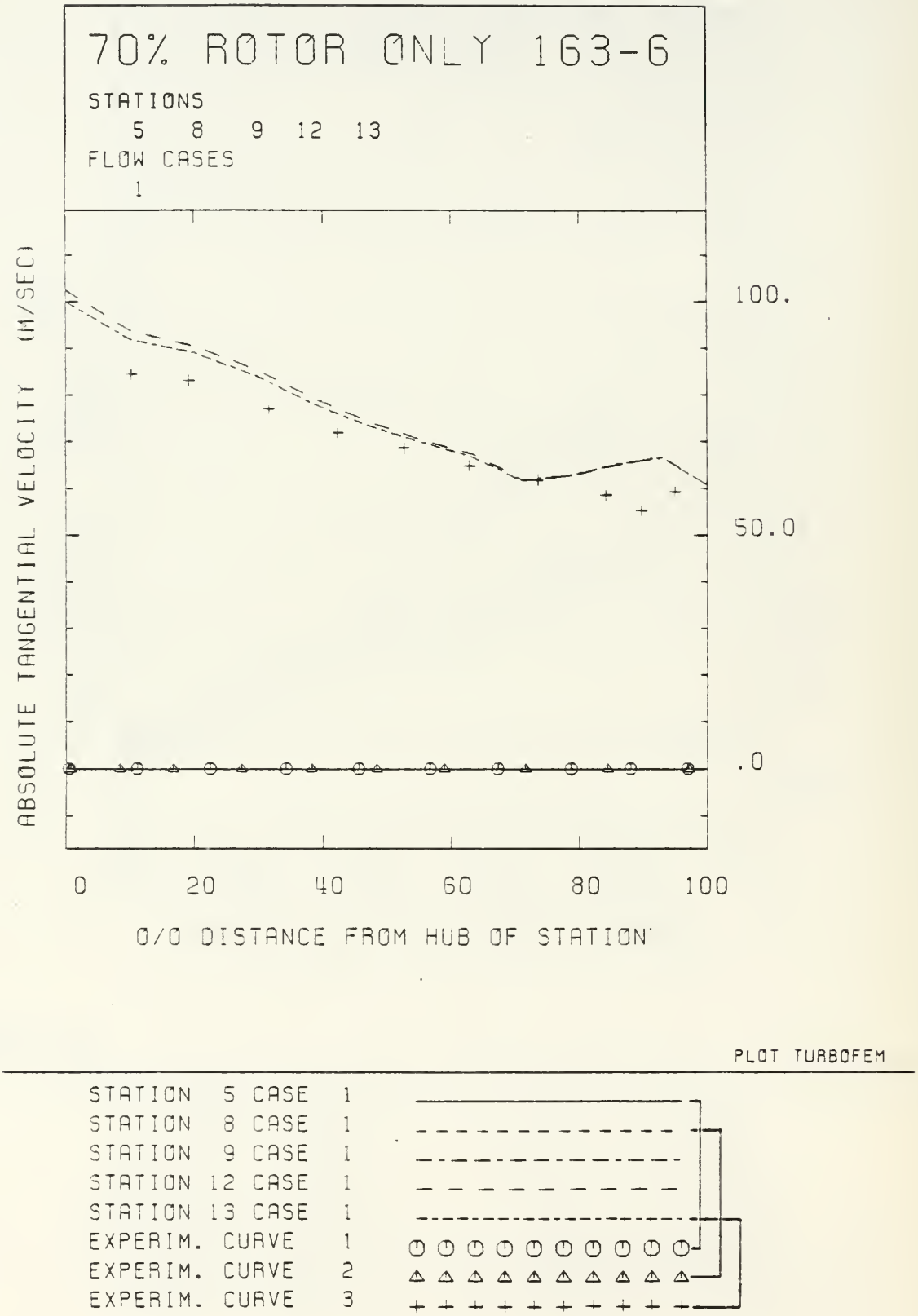

Figure 21. Comparison of measured and calculated absolute tangential velocity component vs blade span at 70% of design speed.

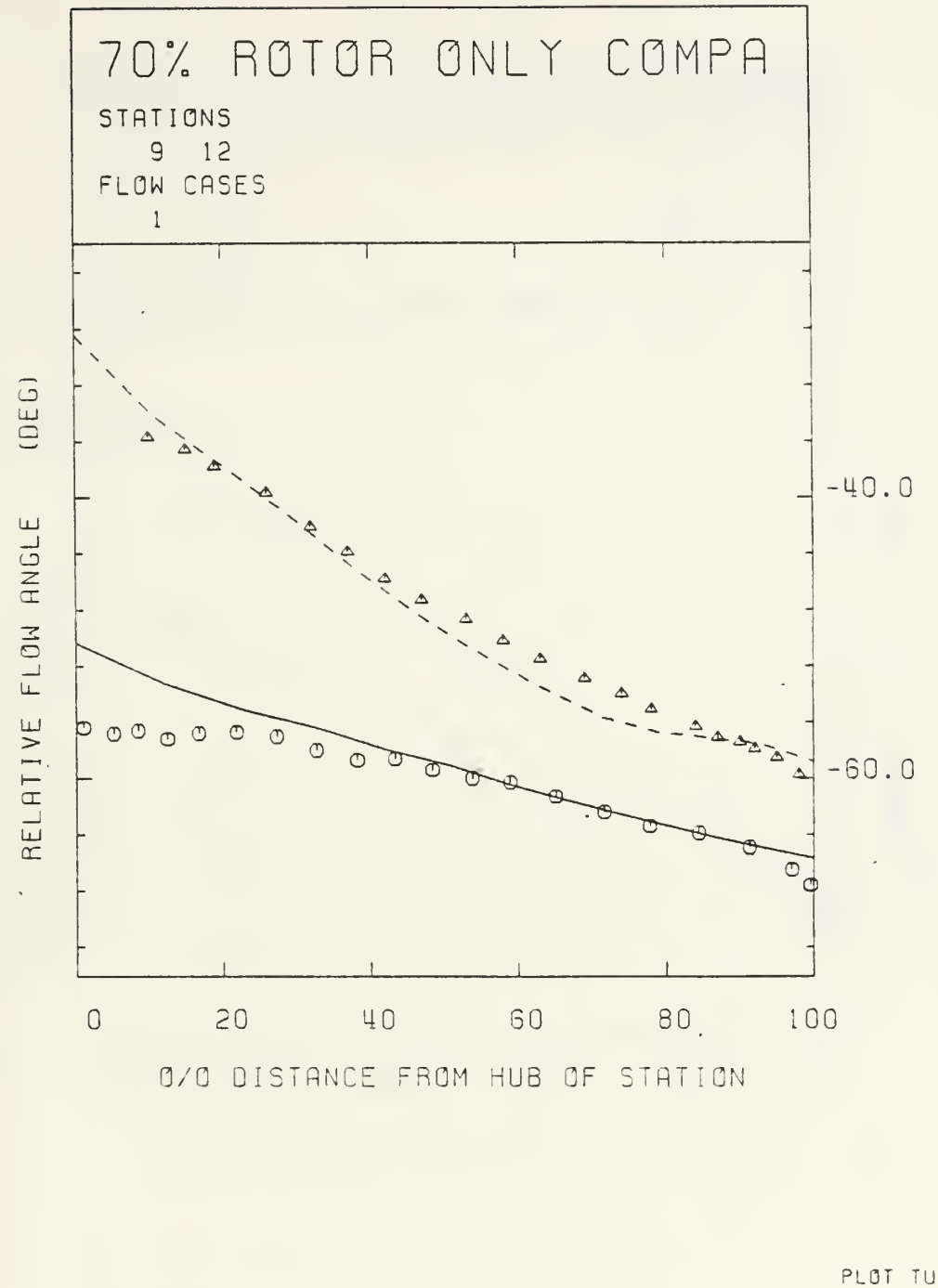

Figure 22. Comparison of measured and calculated relative flow angle vs blade span at 70% of design speed.

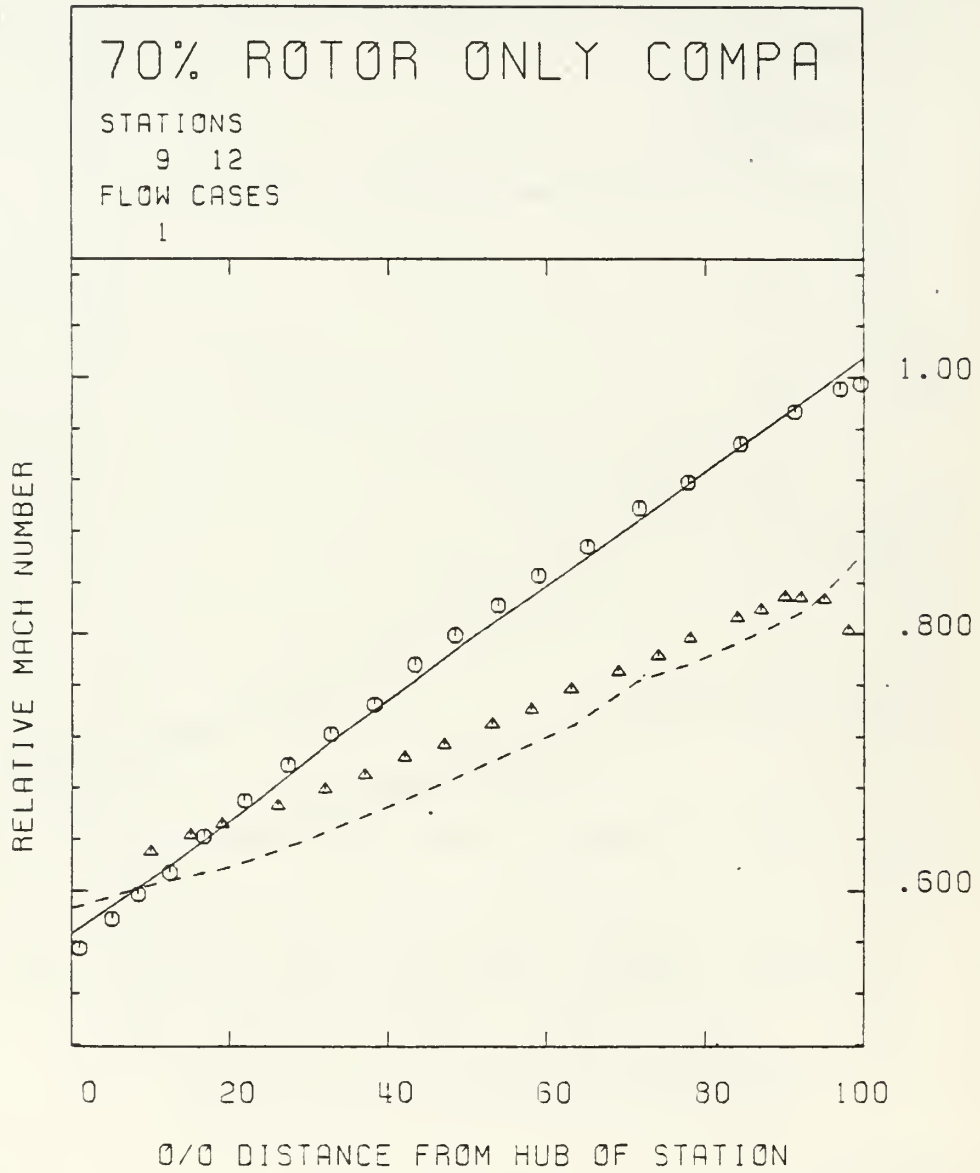

Figure 23. Comparison of measured and calculated relative Mach number vs blade span at 70% of design speed.

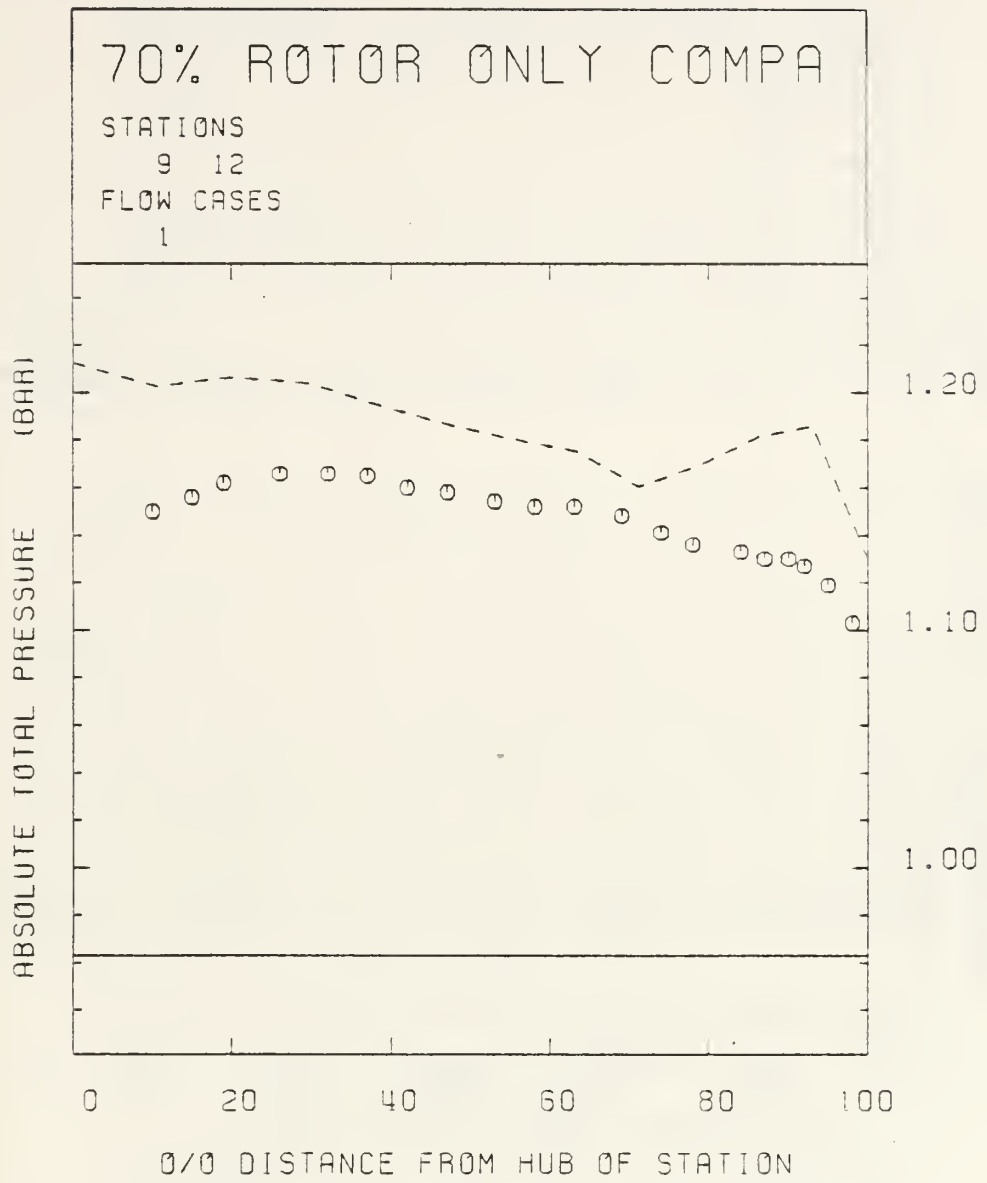

Figure 24. Comparison of measured and calculated absolute total pressure vs blade span at 70% of design speed.

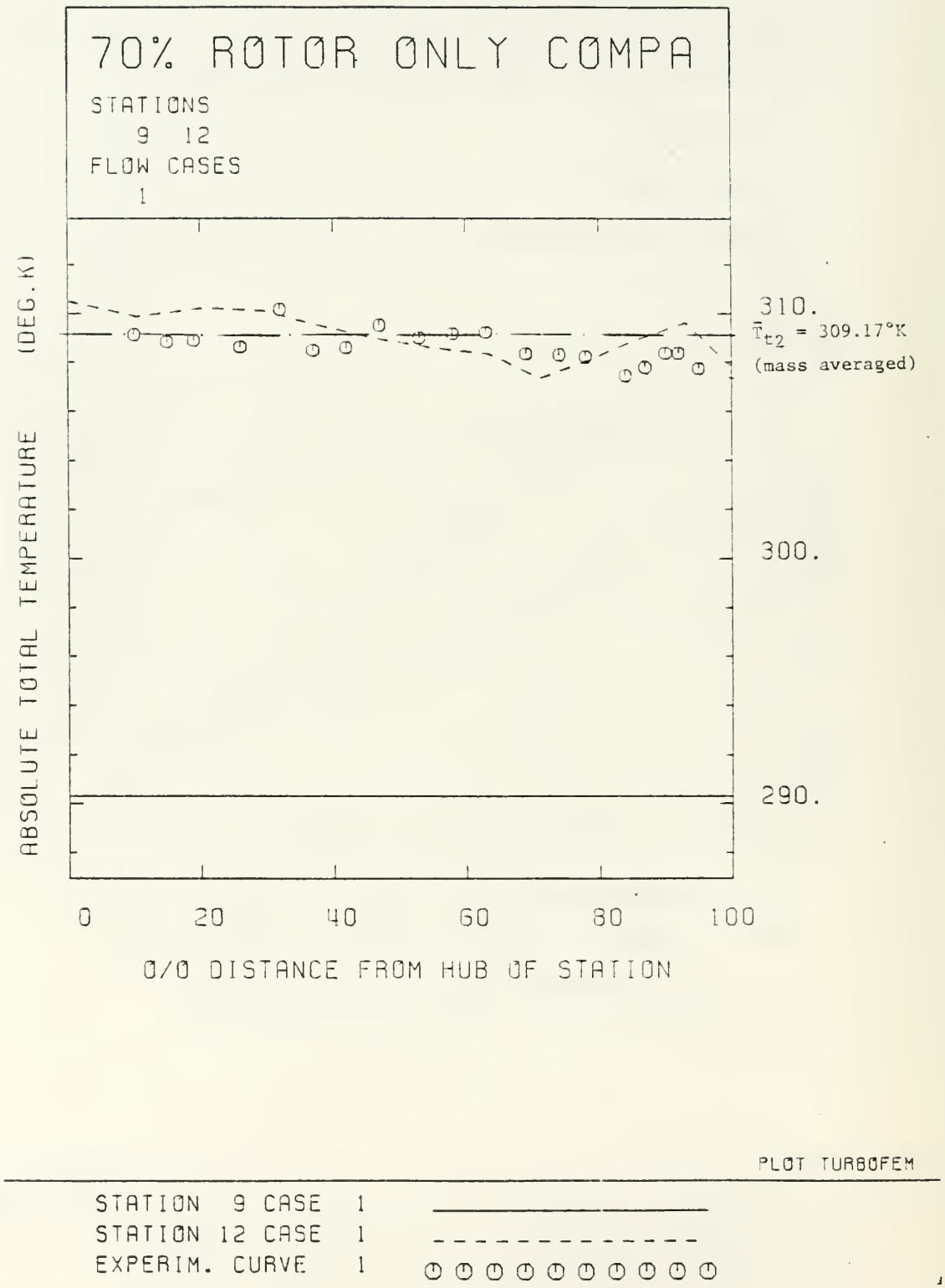

Figure 25. Comparison of measured and calculated absolute total temperature vs blade span at 70% of design speed.

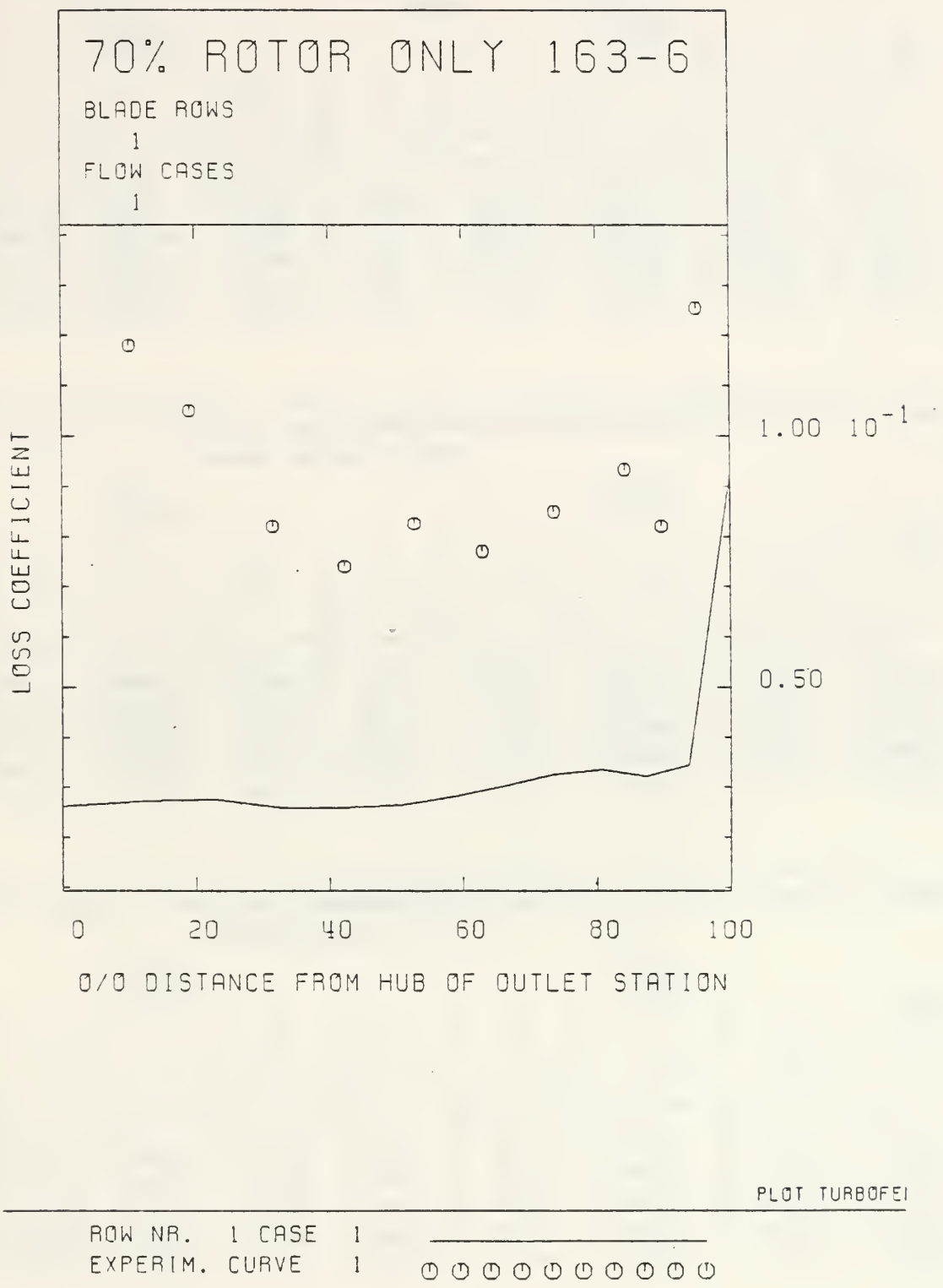

Figure 26. Comparison of measured and calculated loss coefficient vs blade at 70% of design speed.

COMPARISON OF ROTOR AND STATOR INCIDENCE ANGLE

Table I. Data from file T95608 - No honeycomb, large screen, 60% of design speed

	Rotor				Stator			
$\frac{\dot{\Delta m}}{\dot{m}}$ [-]	β_1 [°]	γ [°]	ϕ [°]	i [°]	α_2 [°]	γ [°]	ϕ [°]	i [°]
0.25	50.2	45.06	16.31	5.0	28.0	11.94	38.07	-3.00
0.50	65.2	53.94	11.56	5.7	29.0	12.38	40.94	-3.85
0.75	65.4	58.76	7.04	3.6	24.2	12.87	44.21	-10.78
0.875	64.3	60.27	5.71	2.0	21.9	13.21	46.68	-14.65
1.000	66.4	59.83	4.71	4.1	28.0	14.50	55.60	-14.30

Table II. Data from file T95707 - No honeycomb, no screen, full open throttle, 60% of design speed

	Rotor				Stator			
$\frac{\dot{\Delta m}}{\dot{m}}$ [-]	β_1 [°]	γ [°]	ϕ [°]	i [°]	α_2 [°]	γ [°]	ϕ [°]	i [°]
0.25	57.0	45.06	16.31	3.70	26.5	11.94	38.07	-4.48
0.50	60.2	53.94	11.56	0.00	24.2	12.38	40.94	-8.65
0.75	63.3	58.76	7.04	1.55	22.1	12.87	44.21	-12.88
0.875	65.0	60.27	5.71	2.75	21.3	13.21	46.68	-13.25
1.000	66.9	59.83	4.71	4.55	30.9	14.50	55.60	-11.40

Table III. Data from file T95714 - No honeycomb, no screen, slightly throttled, 60% of design speed

	Rotor				Stator			
$\frac{\dot{\Delta m}}{\dot{m}}$ [-]	β_1 [°]	γ [°]	ϕ [°]	i [°]	α_2 [°]	γ [°]	ϕ [°]	i [°]
0.25	58.3	45.06	16.31	5.09	30.3	11.94	38.07	-0.68
0.50	61.7	53.94	11.56	1.98	28.3	12.38	40.94	-4.55
0.75	64.7	58.76	7.04	2.42	26.0	12.87	44.21	-8.98
0.875	65.6	60.27	5.71	2.48	25.3	13.21	46.68	-11.29
1.000	68.1	59.83	4.71	5.92	37.5	14.50	55.60	-4.80

Table IV. Data from file T92402 - Old bellmouth, no screen, honeycomb, slightly throttle, 60% of design speed

	Rotor				Stator			
$\frac{\dot{\Delta m}}{\dot{m}}$ [-]	β_1 [°]	γ [°]	ϕ [°]	i [°]	α_2 [°]	γ [°]	ϕ [°]	i [°]
0.25	63.1	45.06	16.31	9.9	34.40	11.94	38.07	3.97
0.50	66.2	53.94	11.56	6.5	32.00	12.38	40.94	-0.85
0.75	68.9	58.76	7.04	6.6	29.34	12.87	44.21	-5.64
0.875	70.8	60.27	5.71	7.7	28.00	13.21	46.68	-8.58
1.000	73.5	59.83	4.71	11.3	37.00	14.50	55.60	-5.30

Table V. Data from file T92504 - Old bellmouth, no screen, honeycomb highly throttled, 60% of design speed

	Rotor				Stator			
$\frac{\dot{\Delta m}}{\dot{m}}$ [-]	β_1 [°]	γ [°]	ϕ [°]	i [°]	α_2 [°]	γ [°]	ϕ [°]	i [°]
0.25	67.9	45.06	16.31	14.70	41.7	11.94	38.07	-10.73
0.50	69.5	53.94	11.56	9.78	39.8	12.38	40.94	6.95
0.75	70.4	58.76	7.04	8.12	37.0	12.87	44.21	2.03
0.875	71.9	60.27	5.71	8.78	35.9	13.21	46.68	-0.65
1.000	73.7	59.83	4.71	11.52	44.0	14.50	55.60	-1.70

Table VI. Data from file T95811 - No honeycomb, small screen, open throttle, 60% of design speed

	Rotor				Stator			
$\frac{\dot{\Delta m}}{\dot{m}}$ [-]	β_1 [°]	γ [°]	ϕ [°]	i [°]	α_2 [°]	γ [°]	ϕ [°]	i [°]
0.25	55.8	45.06	16.31	2.7	26.3	11.94	38.07	-4.68
0.50	63.5	53.94	11.56	4.1	26.7	12.38	40.94	-6.15
0.75	64.9	58.76	7.04	2.75	23.8	12.87	44.21	-11.18
0.875	64.6	60.27	5.71	2.25	22.0	13.21	46.68	-14.55
1.000	66.0	59.83	4.71	1.65	31.9	14.50	55.60	-10.40

Table VII. Calculation of stator incidence angle (T95907) 60% of design speed, open throttle

# [-]	H [-]	$\frac{R2}{RO}$ [-]	α2 [°]	γ [°]	ϕ [°]	i [°]	design i [-°]
1	0.000	0.635	27.00	11.568	34.900	-1.99	-0.788
2	0.260	0.730	25.37	11.940	38.069	-5.60	-1.300
3	0.520	0.825	22.50	12.380	40.935	-10.35	-2.200
4	0.756	0.911	20.40	12.866	44.207	-14.57	-3.000
5	0.878	0.955	20.50	13.209	46.681	-16.05	-3.000
6	1.000	1.000	27.00	14.498	55.603	-15.30	0.000

Rotor

# [-]	$\frac{\dot{\Delta m}}{\dot{m}}$ [-]	$\frac{R1}{R2}$ [-]	i [°]
1	0.000	0.5000	3.55
2	0.250	0.6614	2.40
3	0.500	0.7906	0.90
4	0.750	0.9014	1.10
5	0.875	0.9520	1.73
6	1.000	1.0000	2.30

Table VIII. Calculation of stator incidence angle (T95924) 60% of design, speed, closed throttle

# [-]	H [-]	$\frac{R2}{RO}$ [-]	α_2 [°]	γ [°]	ϕ [°]	i [°]	design i [-°]
1	0.000	0.635	39.60	11.568	34.900	10.60	-0.788
2	0.260	0.730	37.54	11.940	38.069	6.56	-1.300
3	0.520	0.825	35.33	12.380	40.935	2.48	-2.200
4	0.756	0.911	33.85	12.866	44.207	-1.12	-3.000
5	0.878	0.955	33.50	13.209	46.681	-3.05	-3.000
6	1.000	1.000	43.60	14.498	55.603	1.30	0.000

Rotor

# [-]	$\frac{\Delta\dot{m}}{\dot{m}}$ equal to H [-]	$\frac{R1}{RO}$ [-]	i [°]
1	0.000	0.5000	8.28
2	0.250	0.6614	6.75
3	0.500	0.7906	4.39
4	0.750	0.9014	4.82
5	0.875	0.9520	5.16
6	1.000	1.0000	6.00

Table IX. Calculation of stator incidence angle (T96013) 70% of design speed, open throttle

# [-]	H [-]	$\frac{R2}{R0}$ [-]	α_2 [°]	γ [°]	ϕ [°]	i [°]	design i [-°]
1	0.000	0.635	26.60	11.568	34.900	-2.40	-0.788
2	0.260	0.730	25.05	11.940	38.069	-5.93	-1.300
3	0.520	0.825	22.91	12.380	40.935	-9.94	-2.200
4	0.756	0.911	21.50	12.866	44.207	-13.47	-3.000
5	0.878	0.955	20.73	13.209	46.681	-15.76	-3.000
6	1.000	1.000	26.00	14.498	55.603	-16.30	0.000

Rotor

# [-]	$\frac{\dot{\Delta m}}{\dot{m}}$ equal to H [-]	$\frac{R1}{R0}$ [-]	i [°]
1	0.000	0.5000	3.53
2	0.250	0.6614	2.89
3	0.500	0.7906	1.15
4	0.750	0.9014	1.25
5	0.875	0.9520	1.92
6	1.000	1.0000	2.50

Table X. Calculation of stator incidence angle (T96023) 70% of design speed, closed throttle

# [-]	H [-]	$\frac{R2}{RO}$ [-]	α_2 [°]	γ [°]	ϕ [°]	i [°]	design i [-°]
1	0.000	0.635	40.00	11.568	34.90	11.00	-0.788
2	0.260	0.730	40.25	11.940	38.069	9.28	-1.300
3	0.520	0.825	37.72	12.380	40.935	4.87	-2.200
4	0.756	0.911	36.00	12.866	44.207	1.03	-3.000
5	0.878	0.955	35.95	13.209	46.681	-0.60	-3.000
6	1.000	1.000	44.00	14.498	55.603	1.70	0.000

Rotor

# [-]	$\frac{\Delta\dot{m}}{\dot{m}}$ equal to H [-]	$\frac{R1}{RO}$ [-]	i [°]
1	0.000	0.5000	9.45
2	0.250	0.6614	6.93
3	0.500	0.7906	4.99
4	0.750	0.9014	4.95
5	0.875	0.9520	5.42
6	1.000	1.0000	6.30

Table XI. Stage full open throttle line

$\frac{N}{N_{ref}}$ [-]	$\dot{m}_{ref}$ [lbs/s]	π [-]	η_{is} [-]	$\frac{\Delta T_t}{T_{t_1}}$ [-]
0.247	5.644	1.021	0.834	0.0073
0.295	6.609	1.030	N/A	N/A
0.326	7.224	1.039	0.856	0.0128
0.400	8.708	1.057	0.865	0.0187
0.494	10.888	1.093	0.872	0.0297
0.590	12.850	1.137	0.878	0.04267
0.623	13.500	1.150	0.858	0.0477
0.656	14.242	1.170	0.868	0.0530
0.683	14.854	1.185	0.860	0.0579

Table XII. Stage, 60% of design speed line

$\frac{N}{N_{ref}}$ [-]	$\dot{m}_{ref}$ [lbs/s]	π [-]	η_{is} [-]	$\frac{\Delta T_t}{T_{t_1}}$ [-]
0.598	12.986	1.141	0.875	0.044150
0.599	13.187	1.141	0.867	0.044509
0.597	13.073	1.144	0.876	0.044796
0.597	13.038	1.149	0.886	0.045820
0.601	12.882	1.153	0.878	0.047344
0.598	12.791	1.156	0.880	0.048176
0.598	12.784	1.162	0.887	0.049713
0.600	12.502	1.162	0.878	0.052158
0.598	12.411	1.176	0.891	0.053385
0.600	12.250	1.183	0.901	0.054873
0.600	12.064	1.188	0.899	0.056233
0.597	11.797	1.192	0.896	0.057650
0.596	11.758	1.198	0.911	0.058433
0.596	11.631	1.202	0.913	0.059349
0.596	11.366	1.204	0.869	0.062835
0.600	11.005	1.217	0.915	0.063295
0.597	10.784	1.219	0.904	0.064592
0.599	11.293	1.211	0.920	0.061215

Table XIII. Stage, 70% of design speed line

$\frac{N}{N_{ref}}$ [-]	$\dot{m}_{ref}$ [lbs/s]	π [-]	η_{is} [-]	$\frac{\Delta T_t}{T_{t1}}$ [-]
0.690	14.95	1.201	0.873	0.06159
0.690	14.82	1.212	0.873	0.06432
0.688	14.58	1.225	0.895	0.06681
0.690	14.50	1.237	0.897	0.07010
0.689	14.153	1.247	0.904	0.07215
0.690	14.053	1.257	0.911	0.07943
0.690	13.723	1.266	0.915	0.07640
0.690	13.542	1.278	0.917	0.07950
0.691	13.322	1.205	0.916	0.08152
0.690	13.168	1.294	0.921	0.08320
0.690	12.850	1.301	0.923	0.08504

Table XIV. Rotor only full open throttle line

$\frac{N}{N_{ref}}$ [-]	m_{ref} [lbs/s]	π [-]	η_{is} [-]	$\frac{\Delta T_t}{T_{t1}}$ [-]
0.248	5.491	1.021	0.793	0.0077
0.295	6.733	1.030	0.820	0.0105
0.329	7.334	1.039	0.852	0.0130
0.395	8.808	1.058	0.886	0.0184
0.493	10.970	1.093	0.913	0.0282
0.524	11.650	1.105	0.907	0.0321
0.556	12.500	1.120	0.916	0.0361
0.589	13.170	1.133	0.913	0.0389
0.590	13.050	1.134	0.918	0.0401
0.620	13.750	1.148	0.927	0.0436
0.654	14.480	1.166	0.926	0.0487
0.687	15.120	1.181	0.904	0.0539

REFERENCES

1. Erwin, J. R., "A Review of the Design of the NPS/TPL Transonic Compressor," Naval Postgraduate School Contractor Report NPS67-83-004CR, March 1983.

2. Neuhoff, F., "Modifications to the Inlet Flow Field of a Transonic Compressor Rotor," Naval Postgraduate School Contractor Report, NPS67-85-008CR, July 1985.

3. Hirsch, IR., C., "Computer Program for Turbomachinery Flows Finite Element Method General Principles," Vrije Universiteit, Brussels, Belgium, 1981.

4. Hirsch, IR., C., "Computer Program for Turbomachinery Flows Finite Element Method User's Guide," Vrije Universiteit, Brussels, Belgium, 1981.

5. Neuhoff, F., "Calibration and Application of a Combination Temperature-Pneumatic Probe for Velocity and Rotor Loss Distribution Measurements in a Compressor," Naval Postgraduate School Contractor Report NPS67-81-03CR, December 1981.

INITIAL DISTRIBUTION LIST

1. Commander
   Naval Air Systems Command
   Washington, DC 20361
   Attention: Code AIR 931 — 1
   Code AIR 931E — 1
   Code AIR 530 — 1
   Code AIR 536 — 1
   Code AIR 5004 — 4
   Code AIR 93D — 1

2. Office of Naval Research
   800 N. Quincy Street
   Arlington, VA 22217
   Attention: Dr. Jack Hansen — 1

3. Commanding Officer
   Naval Air Propulsion Center
   Trenton, NJ 08628
   Attention: G. Mangano, PE-31 — 1

4. Commanding Officer — 1
   Naval Air Development Center
   Warminster, PA 19112
   Attention: AVTD

5. Library — 1
   Army Aviation Material Laboratories
   Department of the Army
   Fort Eustis, VA 23604

6. Dr. Arthur J. Wennerstrom — 1
   AFWAL/POTX
   Wright-Patterson AFB
   Dayton, OH 45433

7. Air Force Office of Scientific Research — 1
   AFOSR/NA
   Bolling Air Force Base
   Washington, DC 20332
   Attention: Dr. James Wilson

8. Mr. P. E. Yaggy — 1
   Director
   U. S. Army Aeronautical Research Laboratory
   AMES Research Center
   Moffett Field, CA 94035

9. Defense Technical Information Center — 2
Cameron Station
Alexandria, VA 22314

10. Naval Postgraduate School
Monterey, CA 93943-51000
Attn: Library (Code 1424) — 1
Professor M. F. Platzer (67Pl) — 1
Turbopropulsion Laboratory (67Sf) — 10